


RESEARCH

Open Access



JMJD6 K375 acetylation restrains lung cancer progression by enhancing METTL14/m6A/SLC3A2 axis mediated cell ferroptosis

Huanxiang Chen¹, Nan Xiao¹, Chenxing Zhang¹, Yang Li¹, Xiangzhuan Zhao¹, Ruike Zhang¹, Lu Bai⁴, Qiaozhen Kang^{3*}, Junhu Wan^{1*}  and Hongyang Liu^{1,2*}

Abstract

Background The Jumonji domain-containing protein 6 (JMJD6), a histone arginine demethylase, is known to have a multifaceted and significant role on cancer progression. However, the specific function and mechanism of JMJD6 in non-small cell lung cancer (NSCLC) have yet to be fully elucidated.

Methods The elevated expression of JMJD6 in lung cancer tissues was confirmed through a combination of bioinformatics and immunohistochemical analysis. Utilizing lung cancer cell lines H460, H157, A549, and H1299, we further investigated the impact of JMJD6 on various cellular processes such as ferroptosis, proliferation, migration, and invasion both in vivo and in vitro. The acetylation of JMJD6 was characterized using immunoprecipitation, co-immunoprecipitation, GST pull down, and immunofluorescence techniques. The regulatory role of JMJD6 acetylation in ferroptosis was assessed by measuring levels of ROS, MDA, and JC-1. WB, qRT-PCR, ChIP and MeRIP techniques were employed to investigate the relationship between the JMJD6 acetylation/METTL14/m6A/SLC3A2 axis.

Results This study revealed elevated levels of JMJD6 in tumor tissue, with high expression correlating strongly with advanced clinical stage in lung cancer patients, and identified JMJD6 as a significantly poor prognostic factor for lung cancer. Functional experiments verified that ectopic overexpression of JMJD6 enhanced the proliferation and migratory capacities of lung cancer cells, while JMJD6 knockdown showed opposite effects. We further find that JMJD6 functions as a negative modulator in regulating ferroptosis process. Mechanistically, JMJD6 affects METTL14 expression in an arginine demethylase dependent manner, and mediates m6A modification of SLC3A2 to regulate its expression level, thereby affecting the sensitivity of lung cancer cells to ferroptosis. Besides, our findings indicate that acetyltransferase p300/CBP associated factor (PCAF) interacts with and acetylates JMJD6 at lysine 375. Acetylation weakens the activity of JMJD6 demethylase, thereby enhancing METTL14 expression and affecting its mediated m6A

*Correspondence:
Qiaozhen Kang
qzkang@zzu.edu.cn
Junhu Wan
wanjh@zzu.edu.cn
Hongyang Liu
hongyangliu@zzu.edu.cn

Full list of author information is available at the end of the article



© The Author(s) 2025. **Open Access** This article is licensed under a Creative Commons Attribution-NonCommercial-NoDerivatives 4.0 International License, which permits any non-commercial use, sharing, distribution and reproduction in any medium or format, as long as you give appropriate credit to the original author(s) and the source, provide a link to the Creative Commons licence, and indicate if you modified the licensed material. You do not have permission under this licence to share adapted material derived from this article or parts of it. The images or other third party material in this article are included in the article's Creative Commons licence, unless indicated otherwise in a credit line to the material. If material is not included in the article's Creative Commons licence and your intended use is not permitted by statutory regulation or exceeds the permitted use, you will need to obtain permission directly from the copyright holder. To view a copy of this licence, visit <http://creativecommons.org/licenses/by-nc-nd/4.0/>.

modification to regulate SLC3A2. Acetylation at lysine 375 also augment the modulation of ferroptosis in lung cancer cells by JMJD6, consequently impeding the lung cancer progression.

Conclusion Taken together, we elucidated the JMJD6 acetylation/METTL14/m6A/SLC3A2 axis as a key mediator of lung cancer progression, indicating that JMJD6 may serve as a potentially prognostic biomarker and therapeutic target for NSCLC.

Keywords JMJD6, Lung cancer, m6A, Ferroptosis, Acetylation

Introduction

Lung cancer is a prevalent malignancy and the leading cause of cancer death worldwide. Approximately 2.2 million new patients are diagnosed with lung cancer every year [1, 2]. According to the histological type of cancer cells, lung cancer is mainly divided into small cell lung cancer (SCLC) and non-small cell lung cancer (NSCLC). NSCLC is the most prevalent form of lung cancer, representing 85–90% of all cases [3]. Treatment options for NSCLC include surgery, radiotherapy, chemotherapy, immunotherapy, and molecular targeted therapy [4–6]. However, a significant number of patients undergoing surgical intervention may experience distant metastasis or local recurrence, resulting in suboptimal treatment outcomes [7–9]. In addition, the majority of individuals diagnosed with cancer are already in advanced stages upon symptom manifestation, leading to poorer treatment responses and shortened survival periods. Therefore, there is a pressing need to delve deeper into alternative molecular pathways involved in the progression of NSCLC and pinpoint novel therapeutic targets to enhance clinical management of lung cancer.

Jumonji domain-containing 6 (JMJD6), a member of the jumonji (JMJC) domain family of histone demethylases, catalyzes the demethylation of H3R2me2 and/or H4R3me2 [10]. The demethylation modification of JMJD6 has been implicated in the regulation of transcription, epigenetics, and various biological processes [10–12]. Numerous studies have demonstrated that dysregulated expression of JMJD6 is associated with the pathogenesis and progression of multiple types of tumors. JMJD6 shaped the pro-tumor microenvironment in breast cancer through ANXA1 dependent macrophage polarization [13]. JMJD6 also exhibits elevated expression levels in clear cell renal cell carcinoma by acting on DGAT1 promoter region, thereby upregulating its expression, which in turn facilitates lipid droplet formation and tumorigenesis [14]. Besides, JMJD6 overexpression has been shown to increase the radiation resistance of hepatocellular carcinoma by activating the ERK pathway through the upregulation of interleukin (IL)-4 transcription. The heightened expression of JMJD6 in lung cancer has been implicated in the regulation of M2-type polarization of tumor-associated macrophages (TAM) via the STAT3/IL-10 signaling pathway [15]. However, the molecular

regulatory mechanism for JMJD6 regulation in lung cancer remains largely unclear.

Recent studies have shown that besides necrosis and apoptosis, there are other novel ways of programmed death with unique biological processes and pathophysiological features. One of them is ferroptosis. Ferroptosis is an iron-dependent process distinct from conventional programmed cell death. The regulation of ferroptosis has focused on the regulation of systemic X_C -system (cysteine/glutamate antiporter system) and GSH metabolism, glutathione (GSH) peroxidase 4 (GPX4) activity, and ROS production [16]. Among them, the X_C -system is located on the cell membrane and mediates the transport of cysteine and glutamate [17–19]. Through system X_C^- , glutamate is transported outside the cell, and the imported cystine participates in GSH production, thereby inhibiting ferroptosis of cancer cells [20]. The X_C^- system belongs to the heterodimeric amino acid transporter (HAT) family and consists of two subunits: the light chain subunit SLC7A11 (xCT) and the heavy chain subunit SLC3A2 (CD98, 4F2hc) [21, 22]. In recent years, many studies have shown that ferroptosis plays an important regulatory role in the occurrence and development of lung cancer progression. For example, m5C methyltransferase NSUN2 can increase the sensitivity of lung cancer cells to ferroptosis activator by reducing the expression of NRF2, thereby inhibiting the progression of lung cancer cells [23]. However, inhibition of RBMS1 in lung cancer cells can inhibit the translation of SLC7A11, reduce the cystine uptake mediated by SLC7A11, and promote ferroptosis in lung cancer cells [24]. In addition, C1q/tumor necrosis factor-related protein-6 (CTRP6) interacts with suppressor of cytokine signaling 2 (SOCS2) in lung cancer cells, leading to the ubiquitination and degradation of SOCS2, which further enhances the downstream xCT/GPX4 signaling pathway [25]. Consequently, there is a growing recognition of the potential efficacy of inducing ferroptosis as a therapeutic approach for tumors. Nevertheless, the association between JMJD6 and ferroptosis in lung cancer cells, as well as the precise underlying molecular mechanisms, remain unexplored and warrant further investigation.

In this study, we verified that JMJD6 is highly expressed in NSCLC and its high expression is closely related to poor prognosis of NSCLC. In addition, we also found that

JMJD6 regulate the demethylation of H4R3me2 in the promoter region of m6A methyltransferase METTL14, thereby affecting its expression. In addition, we found that acetylation weakens the activity of JMJD6 demethylase, thereby regulating METTL14 expression and affecting its mediated m6A modification to regulate SLC3A2, affecting ferroptosis in lung cancer cells. Overall, in this study, we validated the effect of JMJD6 regulation of METTL14 on SLC3A2 m6A levels, which in turn affects SLC3A2 expression and ultimately ferroptosis in NSCLC. The discovery of this regulatory process further improves the research on the molecular mechanism of lung cancer progression, and brings new targets and therapeutic strategies for the treatment of lung cancer.

Materials and methods

Cell culture, reagents and antibodies

Human NSCLC cell lines H460 (RRID: CVCL_0459), H157 (RRID: CVCL_0463), A549 (RRID: CVCL_0023), H1299 (RRID: CVCL_0060) and human normal lung epithelial cell line BEAS-2B (RRID: CVCL_0168) were purchased from the Wuhan Pricella Biotechnology Co., Ltd. All cell lines were cultured in 5% CO₂ at 37 °C in a humidified incubator. RRID: CVCL_0168 and RRID: CVCL_0023 were cultured in DMEM medium. RRID: CVCL_0463, RRID: CVCL_0060, and RRID: CVCL_0459 were cultured in RPMI-1640. Both DMEM and RPMI-1640 were supplemented with 10% (vol/vol) fetal bovine serum (FBS) and 1% penicillin/streptomycin. The antibodies used in this study were listed as follows: JMJD6 antibody (Santa Cruz Biotechnology, Cat# sc-28348, 1:1000), METTL14 antibody (CST, Cat# 48699, 1:1000), SLC3A2 antibody (Abways, Cat# CY8416, 1:1000), GAPDH antibody (Abways, Cat# AB2000, 1:6000), Flag-tag antibody (Abways, Cat# AB0030, 1:1000), HA-tag antibody (proteintech, Cat# 51064-2-AP, 1:3000), Acetylated-Lysine Antibody (CST, Cat# 9441, 1:1000), JMJD6-acK375 antibody (Jiaxuan Biotech Cat#JXR7611, 1:1000), Rabbit Anti-Goat IgG (H+L) HRP (Abways, Cat# AB0101, 1:8000).

Clinical samples

The specimens were obtained with the written informed consent of all patients. And has won The First Affiliated Hospital of Zhengzhou University Scientific Research and Clinical Trials Ethical Committee approval, project number is 2020 - KY - 301.

Quantitative real-time PCR (RT-qPCR)

Total RNA was extracted from cultured cells using the total RNA extraction re-agent Beyozol (Beyotime R0011) according to the manufacturer's instructions. RNA purity and content were determined using a NanoDrop 2000c spectrophotometer (ThermoFisher Scientific). 1

ug of total RNA was reverse transcribed according to Hifair®III 1st Strand cDNA Synthesis SuperMix for qPCR (YEASEN 11141ES60). Real-time quantitative PCR reactions were then performed using SYBR Green Master Mix (YEASEN 11202ES08) on a QuantStudio 3 detection system (ThermoFisher Scientific). JMJD6 specific primers for: forward primer 5'-AAACTTTTGGGAAGACTACAAGGTGC-3'; reverse primer 5'-CCCAGAGAGGGTCGATGTGAATC-3'. SLC3A2 specific primers for: forward primer 5'-CTGGTGCCGTGGTCATAATC-3'; reverse primer 5'-GCTCAGGTAATCGAGACGCC-3'. METTL14 specific primers for: forward primer 5'-GAGATTGCAGCACCTCGATC-3'; reverse primer 5'-TGCTACGCTTCACAGTTCCT-3'.

Cell proliferation, migration and invasion assays

Cell proliferation was detected by colony formation assay, CCK8 and EdU assay. Colony formation assay: 700 cells were added to each well of a 6-well plate and cultured for about 2 weeks until obvious colony formation appeared. The cells were gently washed with PBS, fixed with 4% paraformaldehyde, stained with crystal violet (Beyotime), and the number of colonies was counted. For CCK8 assays, the results were performed according to the CCK-8 Cell Proliferation Kit (US EVERBRIGHT); at each time point, 10 µl of CCK-8 was added to each well of a 96-well plate and the cells were stained at 37 °C. The absorbance was then measured at 450 nm. EdU experiments, EdU experiments were performed using the BeyoClick EdU cell proliferation kit (Beyotime) containing Alexa Fluor 488 and were performed according to the manufacturer's instructions.

Cell migration and invasion assay: For wound healing assay, the cells were spread into a 3.5 cm culture dish in advanced stage. When the cell confluence reached more than 90%, 3 wounds were scratched with 10ul sterile tips, the floating cells were washed off with PBS, and then the cells were cultured in serum-free medium for 12 h. For the transwell assay, lung cancer cells of different transfection groups were suspended in 200ul serum-free medium at a concentration of 1×10^5 cells /ml and placed in the upper chamber of the transwell chamber. For invasion assays, inserts were precoated with 100ul of diluted Matrigel for 30 min, and 600ul of medium containing 20% FBS was added to the lower chamber of the transwell apparatus. The cells were incubated for 6 to 8 h for migration assay and 24–48 h for invasion assay. After incubation, inserts were washed with PBS, fixed in 4% formaldehyde for 20 min, and stained with crystal violet for 30 min.

Cell viability and MDA

Cells were first seeded in 96-well plates and treated with Erastin (MedChemExpress, #HY-15763) or Ferrostatin-1

(MedChemExpress, # HY-100579). The cells were then incubated with 10 μ L of CCK8 (US EVERBRIGHT) at 37 °C for 30–40 min, and finally the absorbance at 450 nm was measured by enzyme labeling. Malondialdehyde (MDA) detection kit (Beyotime, #S0131S) was used to analyze the production of MDA in lung cancer cells of different transfection groups. In this experiment, erastin was used at a concentration of 25 μ M for 48 h. ferrostatin-1 was used at a concentration of 20 μ M for 48 h.

ROS and JC-1 assays

JC-1 was detected using a mitochondrial membrane potential detection kit (Beijing Solarbio Science&Technology Co.,Ltd, #M8650). The cells were pre-seeded in glass-bottom cell culture dishes. After the cells were completely attached to the wall, the laser confocal detection (Carl Zeiss AG, ZEISS LSM 880) was performed according to the instructions. Under normal conditions, the mitochondria were in the multimolecular state and emitted red fluorescence (excitation wavelength 585 nm, emission wavelength 590 nm). When apoptosis occurred, JC-1 was in a monomeric state and produced green fluorescence (excitation wavelength 514 nm, emission wavelength 529 nm).

ROS levels were measured using the Reactive oxygen Species Detection kit (Beyotime, #S0033S). After the fluorescent probe DCFH-DA enters the cells, intracellular reactive oxygen species can oxidize non-fluorescent DCFH to produce fluorescent DCF, and the intracellular ROS content can be reflected by detecting the fluorescence of DCF. Assays were performed using a flow cytometer (BD ACCURI C6 PLUS) and data were analyzed using FlowJo (RRID: SCR_008520). In both experiments, erastin was used at a concentration of 25 μ M for 48 h. ferrostatin-1 was used at a concentration of 20 μ M for 48 h.

Immunoprecipitation (IP) and Co-IP

For IP and Co-IP, cells were first lysed in RIPA containing deacetylase inhibitors and protease inhibitors, Anti-Flag affinity purified gel beads were added and incubated overnight at 4 °C with shaking. After centrifugation, the precipitate was collected and washed three times with lysis buffer. 2Xloading buffer was added and boiled for 8 min. The boiled compounds were centrifuged again, and the supernatant was used for subsequent Western blotting. For the pan acetylation analysis, the acetylated lysine antibody (CST, Cat# 9441, 1:100) was added to the cleavage product along with protein A beads, and the bed was shaken overnight at 4 °C.

GST pull-down assays

The GST-PCAF fragment protein was induced in BL21 strain and extracted by ultrasound. Then, GST Sep

Glutathione Agarose Resin (YEASEN, #20507ES10) was added and purified by shaking overnight at 4 °C. GST-empty or GST-PCAF fragment proteins were added to 8 μ g Flag-JMJD6 transfected cell lysates, shaken for 6 h at 4 °C, centrifuged, and beads eluted with 2Xloading buffer. The protein expression was detected by SDS-polyacrylamide gel electrophoresis and Western blotting.

Chromatin immunoprecipitation (ChIP) assay

H1299 was cross-linked with 1% formaldehyde for 10 min, the reaction was terminated using glycine buffer, and cells were lysed by sonication for 5 min at 4 °C. The obtained DNA fragments were confirmed by agarose gel electrophoresis. After confirmation, immunoprecipitation was performed with the use of the ChIP Assay Kit (Beyotime, P2078) according to the manufacturer's instructions. Samples were finally treated with RNase A and proteinase K before RT-qPCR analysis.

MeRIP assays

Total RNA was extracted with Beyozol (Beyotime R0011) and DNA was removed with DNase. m6A RNA enrichment kits (Epigentek, USA) were used for the MeRIP assay according to the manufacturer's instructions. The m6A-containing target fragment is pulled down using beads conjugated to the m6A capture antibody, and the RNA sequences at the ends of the m6A-containing region are cleaved using a lysase mixture. The enriched RNA is then released, purified and eluted, and RT-qPCR is performed after MeRIP to quantify changes in m6A methylation of the target gene.

Immunofluorescence and immunohistochemistry staining

Tissue sections were fixed in formaldehyde, dehydrated in xylene, antigen repaired in sodium citrate, and removed in hydrogen peroxide. Sections were incubated with primary antibodies against JMJD6(1:200), GPX4(1:200), SLC3A2(1:200), xCT(1:200), and JMJD6-ackK375 (1:200) overnight at 4 °C. Sections were treated with secondary antibodies for 1 h at room temperature and examined by the streptavidin-biotin-peroxidase method. The IHC results were analyzed and scored by pathologists. For immunofluorescence, cells were fixed with 4% formaldehyde, permeabilized and blocked, and then stained with anti-Flag-tag (1:500), JMJD6-ackK375(1:500) primary and fluorescent secondary antibodies (Alexa Fluor 594-labeled goat anti-rabbit IgG) and DAPI as indicated. Finally, the images were taken with a laser confocal microscope.

In vivo xenograft tumor growth experiments

Balb/c nude mice were subcutaneously injected with 1×10^6 stable H1299 cells in the lateral abdomen. Tumor size was measured at the indicated times. Eighteen days



(See figure on previous page.)

Fig. 1 JMJD6 expression is upregulated and associated with poor prognosis in Lung cancer patients. **(A)** TIMER 2.0 database was used for pan-cancer analysis of JMJD6. **(B)** The relative expression levels of JMJD6 in lung cancer tissues and adjacent normal tissues in TCGA database. **(C)** Accuracy of assignment with paired tumor and normal samples from TCGA lung cancer cohort. **(D, E)** CPTAC data analysis showed that the expression level of JMJD6 in lung cancer tissues was significantly higher than that in normal tissues **(D)**. Moreover, elevated JMJD6 expression level was significantly correlated with higher tumor grade of lung cancer **(E)**. **(F)** Kaplan-Meier analysis of the TCGA dataset showed that high JMJD6 expression predicted poor overall survival. log-rank test, $P=0.0021$. **(G)** The Kaplan-Meier survival analysis was used to analyze the prognosis of JMJD6 in lung cancer from TCGA and GEO database. P values were determined by log-rank test ($P=1.2e-05$). **(H, I, J)** Kaplan-Meier survival analysis of stage I, II and III lung cancer patients using TCGA database. **(K)** The expression of JMJD6 in paired normal lung tissues and lung cancer tissues was analyzed by immunohistochemistry, and the quantitative results of immunohistochemical scores are on the right. **(L)** RT-qPCR was used to analyze the expression levels of JMJD6 in four different lung cancer cell lines and normal lung epithelial cell BEAS-2B, and statistical analysis was performed. **(M)** Cell annotated t-SNE plot, with different coloured dots representing the different cell type information annotated. **(N)** Tumour cell clustering t-SNE plot, 0–4 represent 5 different cell clusters, respectively. **(O)** Heatmap showing expression of significantly upregulated top5 marker genes in 5 different clusters of tumour cells. **(P)** Violin plots showing JMJD6 gene expression in various tumour cell subpopulations. Data are expressed as mean \pm SD. * $p < 0.05$; ** $p < 0.01$; *** $p < 0.001$

after implantation of lung cancer cells, 30 mg/kg of Eras-tin was injected in situ as directed, once every three days. Tumor diameters were recorded at 5-day intervals starting when the tumor was visible and detectable. When the tumor diameter reached about 1 cm, the tumor was dissected and the tumor weight was measured.

Statistical analysis

All experiments were made in triplicate, and GraphPad Prism (RRID: SCR_002798) software was used for statistical analysis. Data are presented as mean \pm standard deviation (SD). The T test was used for comparison between groups. Overall survival with Kaplan Meier - method to evaluate, the log - rank test to determine the difference was statistically significant. * Indicates $p < 0.05$; ** indicates $p < 0.01$; *** indicates $p < 0.001$.

Results

JMJD6 expression is upregulated and associated with poor prognosis in lung cancer patients

JMJD6 has been identified as exhibiting high levels of expression in a range of tumor types [14, 15, 26, 27], yet its expression in lung cancer and the specific mechanism are still not very clear. In order to further explore the role of JMJD6 in the occurrence and development of lung cancer, we conducted a systematic bioinformatics analysis using multiple authoritative databases. Firstly, based on the Cancer Genome Atlas (TCGA) database, the expression situation of JMJD6 at the pan-cancer level was preliminarily analyzed (Fig. 1A). The results show that JMJD6 is significantly highly expressed in multiple cancer types, including lung cancer, which provides important clues for subsequent studies focusing on lung cancer.

Then, based on the TCGA database, a more refined differential expression analysis was performed to accurately compare the expression levels of JMJD6 in lung cancer tissues and normal tissue samples (Fig. 1B and C). The results showed that the expression level of JMJD6 was significantly increased in lung cancer tissues compared with normal tissues. In order to further enhance the reliability of the results, the Clinical Proteomics in Cancer Analysis Consortium (CPTAC) database was introduced

to further explore the expression of JMJD6 in lung cancer and its corresponding normal tissues (Fig. 1D). The results of CPTAC database analysis were in high agreement with the previous TCGA database finding that JMJD6 was stably overexpressed in lung cancer tissues. Moreover, using the rich resources of CPTAC database, we further explored the intrinsic association between JMJD6 expression and tumor stage (Fig. 1E), and found a significant positive correlation between elevated JMJD6 expression and higher tumor grade.

Considering that the prognosis of patients is the focus of clinical attention, this study also comprehensively evaluated the survival information of JMJD6 in lung cancer by integrating TCGA and GEO databases (Fig. 1F and G). The comprehensive analysis results showed that high expression of JMJD6 often predicted poor prognosis of lung cancer patients, and provided a potential new indicator for clinical prognosis judgment. In order to further analyze the correlation between the poor prognosis caused by JMJD6 high expression and the Stage of lung cancer patients, we performed a more detailed survival analysis for stage I-III lung cancer patients. After rigorous statistical processing, it was found that the high expression of JMJD6 was significantly correlated with the prognosis of patients in the Stage I patient population, and the prognosis of patients with high expression of JMJD6 was significantly worse (Fig. 1H), suggesting that this gene may play a key role in the progression of early lung cancer. Similarly, high expression of JMJD6 may still be an important risk factor for poor prognosis in Stage II patients (Fig. 1I), further confirming its negative prognostic effect in the course of lung cancer. However, in patients with Stage III, the effect of JMJD6 high expression on the prognosis of patients is relatively insignificant (Fig. 1J), which may be related to the complex biological characteristics of tumors in this stage, the superposition effect of multiple therapeutic interventions, and the heterogeneity of samples. Further research is needed to clarify the underlying mechanism.

To further investigate the expression of JMJD6 in lung cancer, we performed immunohistochemical staining (IHC) on 25 cancerous tissues and 25 normal lung

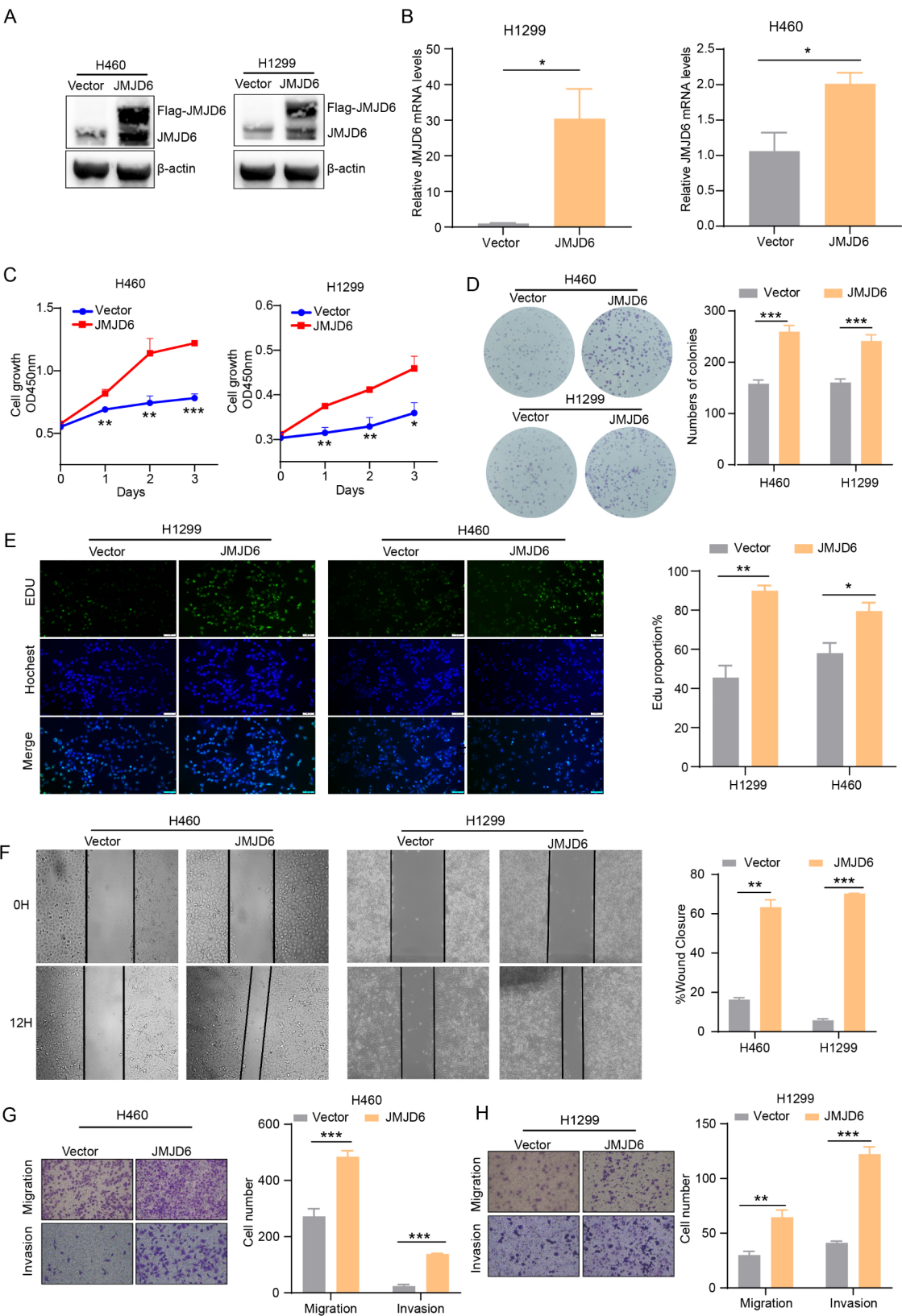


Fig. 2 (See legend on next page.)

(See figure on previous page.)

Fig. 2 JMJD6 overexpression stimulates NSCLC progression in vitro. **(A)** Western blot and **(B)** RT-qPCR were used to verify the overexpression of JMJD6 in H460 and H1299 cells at the mRNA and protein levels, respectively. **(C)** CCK-8 was used to detect the effect of JMJD6 overexpression on cell proliferation in H460 and H1299 cell lines. **(D)** Colony formation assay and **(E)** EdU were also used to detect the effect of JMJD6 overexpression on cell proliferation in H460 and H1299 cell lines. Representative images are shown on the left and statistical data analysis on the right. **(F)** The migration ability of H460 and H1299 cells after overexpression of JMJD6 was determined by wound healing assay. Representative images are shown on the left and statistical data analysis on the right. **(G, H)** Transwell assay was used to detect the effect of JMJD6 overexpression on the migration and invasion of H460 and H1299 cells. Representative images are shown on the left and statistical data analysis on the right. Data are expressed as mean \pm SD. Scale bars represent 100 μ m. * p < 0.05; ** p < 0.01; *** p < 0.001

tissues. The expression of JMJD6 was assessed using a scoring system ranging from 0 to 12 points based on the intensity of staining and the percentage of cells presenting a significant positive reaction. The results of the study also showed that the expression level of JMJD6 was significantly elevated in lung cancer tissues compared to normal lung tissues (Fig. 1K). In addition, the expression of JMJD6 was relatively higher in lung cancer cell lines H1299 and H460 compared with normal lung epithelial cells BEAS-2B, while the expression was higher in cell lines A549 and H157 (Fig. 1L).

Single-cell resolution helps us to better understand the diversity of tumor cell subgroups. Therefore, we sought to determine whether it is possible to distinguish differences in JMJD6 expression in different lung cancer cell subgroups at the single-cell level. We selected the GEO: GSE117570 dataset for analysis. The data were first filtered, standardized and normalized. Then, high variant genes in single-cell data were subjected to principal component downscaling (Fig. S5A) and available dimension filtering (Fig. S5B). Subsequently, cells were analyzed for overall clustering using the FindClusters function (Fig. S5C). Each cell cluster was manually annotated based on classical marker genes (Fig. 1M). A total of six major cell types were annotated, namely epithelial cells, T cells, NK cells, myeloid cells, B cells and other cell types. Heatmaps were calculated and plotted using the FindAllMarkers function, showing the relative expression levels of the top five (Top5) marker genes for each annotated cell (Fig. S5D). To further explore the heterogeneity of non-small cell carcinoma tumor cells and the distribution of JMJD6 genes in different tumor cell subgroups. All epithelial cells were extracted from the overall cells using the subset function and the analysis process from data normalization to dimensionality reduction clustering was repeated. The results showed that 1320 tumor cells could be classified into 5 clusters (Fig. 1N). Significantly highly expressed genes in each subgroup were annotated immediately afterward with a threshold of $\log_{2}FC = 0.25$ (Fig. 1O and S5E). We further focused on the expression of JMJD6 genes in each tumor cell subgroup and plotted violin plots (Fig. 1P) and bubble plots (Fig. S5F) for demonstration. The results showed that the expression of JMJD6 varied in different tumor cell subgroups. JMJD6 was significantly highly expressed in the C0 and C1 subgroups, while it was significantly less expressed in the C2

and C3 subgroups. These results suggest that JMJD6 is upregulated in lung cancer and that there is a potential link between high expression levels of JMJD6 and poor prognosis. And there is heterogeneity in the expression of JMJD6 in lung cancer cells.

JMJD6 overexpression stimulates NSCLC progression in vitro

To evaluate the biological significance of JMJD6 in lung cancer progression, we initially established stable lung cancer cell lines overexpressing JMJD6 in H1299 and H460 cells with relatively low expression levels of JMJD6. The upregulation of JMJD6 expression in H1299 and H460 cell lines at both the mRNA and protein levels was confirmed using real-time quantitative PCR (RT-qPCR) and Western blot (Fig. 2A and B). The impact of JMJD6 on lung cancer cell proliferation, migration, and invasion was examined through in vitro functional assays. The results of the CCK-8 cell proliferation assay indicated a significant increase in proliferation rate in the H1299 and H460 cell lines following JMJD6 overexpression (Fig. 2C). Furthermore, the colony formation assay demonstrated a marked increase in the number of cell colonies in the JMJD6 overexpression group compared to the control group (Fig. 2D). Since the cell proportion of EdU is an important measure of cell proliferation rate, we also performed EdU experiments (Fig. 2E). The results showed that overexpression of JMJD6 resulted in a higher proportion of cells incorporated with EdU, indicating an enhanced rate of cell proliferation. Subsequent investigation using a wound healing assay confirmed that JMJD6 overexpression promoted the migration of lung cancer cells, as evidenced by accelerated wound closure compared to control cells (Fig. 2F). Transwell assay was employed to assess the migration of lung cancer cells, and Matrigel treatment in the chamber was utilized to evaluate their invasive potential (Fig. 2G and H). The conclusive findings indicated a notable increase in the invasion and migration capabilities of lung cancer cells within the JMJD6 overexpression cohort. These results imply that elevated JMJD6 expression facilitates tumorigenesis in lung cancer by augmenting cellular proliferation, migration, and invasion, thus indicating a potential oncogenic function for JMJD6.

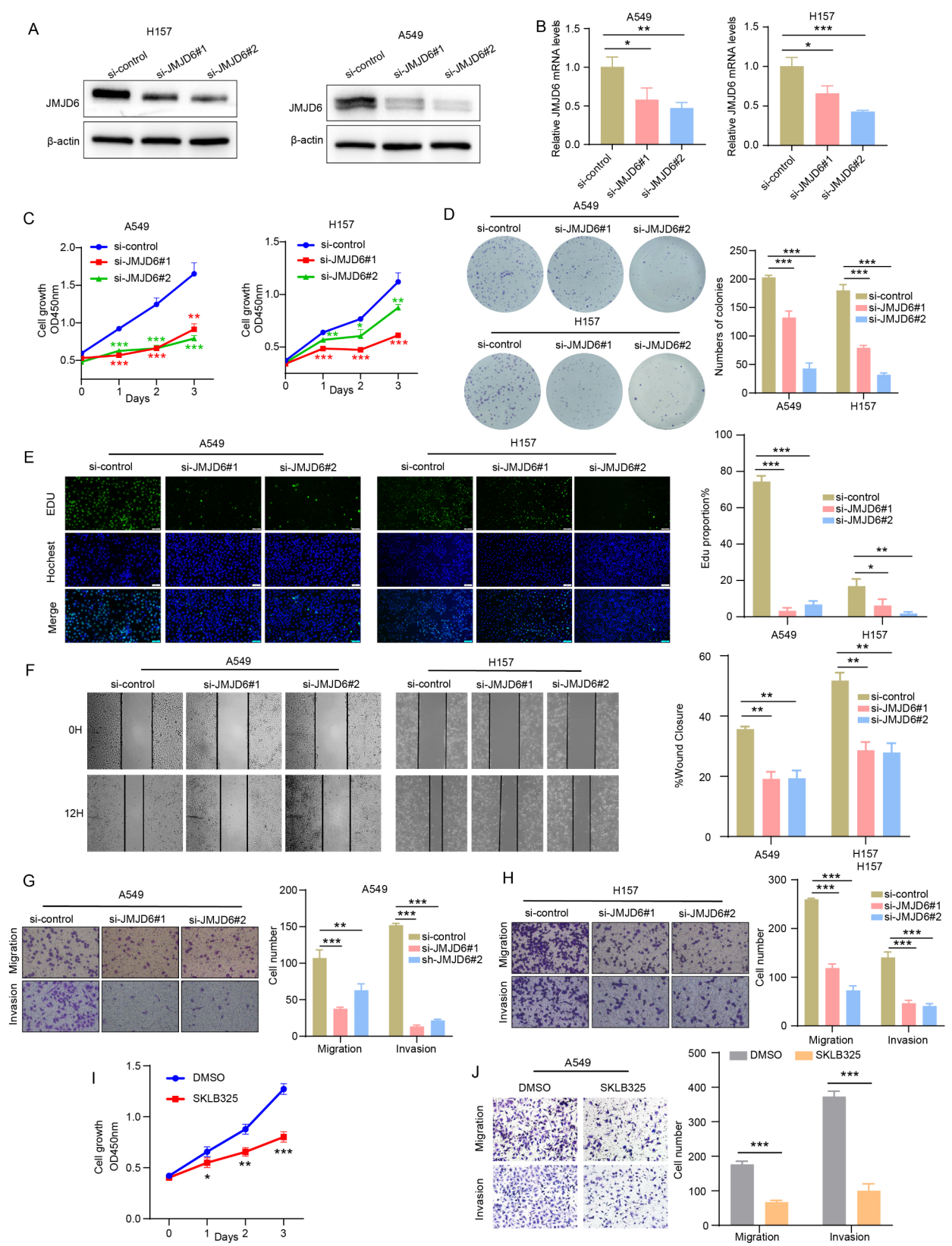


Fig. 3 (See legend on next page.)

(See figure on previous page.)

Fig. 3 JMJD6 deficiency significantly represses NSCLC progression in vitro. **(A)** Western blot and **(B)** RT-qPCR were used to detect the knockdown efficiency of JMJD6 in A549 and H157 cell lines at protein and mRNA levels, respectively. **(C)** CCK-8 assay was used to detect the effect of JMJD6 knockdown on the proliferation of H157 and A549 cells. **(D)** Colony formation assay and **(E)** EdU were also used to detect the effect of JMJD6 knockdown on the proliferation of H157 and A549 cells. Representative images are shown on the left and statistical data analysis is shown on the right. **(F)** The effect of JMJD6 knockdown on the migration ability of A549 and H157 cells was detected by wound healing assay. Representative pictures are shown on the left and statistical data analysis on the right. **(G, H)** The effect of JMJD6 knockdown on the migration and invasion ability of A549 **(G)** and H157 **(H)** cells was detected by transwell. Representative pictures are shown on the left and statistical data analysis on the right. **(I)** The effect of JMJD6 inhibitor SKLB325 on the proliferation of A549 cells was detected by CCK-8 cell proliferation assay. **(J)** Transwell assay was used to detect the effect of JMJD6 inhibitor SKLB325 on the migration and invasion of A549 cells. Data are expressed as mean \pm SD. Scale bars represent 100 μ m. * $p < 0.05$; ** $p < 0.01$; *** $p < 0.001$

JMJD6 deficiency significantly represses NSCLC progression in vitro

To further confirm the regulatory function of JMJD6 in lung cancer progression, A549 and H157 cells with relatively high expression of JMJD6 were transfected with lentivirus to knockdown JMJD6, and stable knockdown cell lines were established. The efficacy of JMJD6 knockdown was confirmed at both the mRNA and protein levels using RT-qPCR and Western blot analysis, respectively (Fig. 3A and B). Subsequently, the CCK-8 cell proliferation assay was conducted, and the results showed that suppression of JMJD6 expression in these cell lines led to a decreased proliferation rate compared to their respective controls (Fig. 3C). Colony formation assay (Fig. 3D) and EdU assay (Fig. 3E) were used to further investigate the effect of JMJD6 on the proliferation of NSCLC cells. The findings revealed a decrease in the number of EdU-labelled proliferating cells and a significant reduction in cell colonies upon inhibition of JMJD6 expression, suggesting a notable attenuation in the proliferation capacity of lung cancer cells in the absence of JMJD6. Furthermore, the study also assessed the influence of JMJD6 on the migration and invasion of NSCLC cells. The results from both wound healing (Fig. 3F) and transwell (Fig. 3G and H) assays demonstrated a significant reduction in the migratory capacity of A549 and H157 cells following JMJD6 inhibition compared to the control group. Additionally, the invasive potential of lung cancer cells was evaluated using Matrigel treatment in the transwell assay, revealing a decrease in the number of invasive cells upon JMJD6 knockdown. In conclusion, these results indicate that JMJD6 knockdown effectively impedes the progression of NSCLC in vitro.

To further validate our results and enhance the clinical translation of our findings. We also selected SKLB325, a small molecule inhibitor of JMJD6, based on previous studies of JMJD6-related inhibitors [28, 29], and purchased the finished drug from MCE. The anti-tumor effect of JMJD6 deficiency was further confirmed by partial in vitro functional experiments using SKLB325 in A549 and H1299 cell lines. CCK-8 cell proliferation assay (Fig. 3I and S1C) was performed in A549 and H1299 cell lines, and the results showed that the proliferation rate of both cell lines decreased significantly after treatment with SKLB325 inhibitor. In addition, transwell cell

migration (Fig. 3J and S1D) and invasion assays (Fig. 3J and S1D) were performed, and the results proved that the migration and invasion abilities of both cell lines were significantly decreased after treatment with SKLB325. The above results again demonstrated that inhibition of JMJD6 expression has a significant inhibitory effect on lung cancer cell progression in vitro. It also suggests the further development of small molecule inhibitors targeting JMJD6 and its role in the progression of different cancers.

JMJD6 functions as a negative modulator in regulating lung cancer cell ferroptosis

To explore the role of JMJD6 in lung cancer progression and its effect on downstream target genes, we performed RNA-seq analysis in H1299 cells transfected with JMJD6 overexpression. The sequencing data were analyzed by principal component analysis (PCA) (Fig. 4A) and unsupervised hierarchical clustering analysis (unsupervised hierarchical clustering) (Fig. 4B), respectively. Subsequently, significantly differentially expressed genes (DEGs) were divided into up-regulated genes and down-regulated genes for Gene ontology (GO) (Fig. 4C) and Kyoto Encyclopedia of Genes and Genomes (KEGG) (Fig. 4D) analyses. The results show that JMJD6 is involved in a variety of signal transduction and cell adhesion related signaling pathways, which is closely related to the occurrence, development and metastasis of tumors. Notably, some of the DEGs that were negatively correlated with ferroptosis, such as SLC3A2, were up-regulated when JMJD6 expression was changed, so it was enriched in the up-regulated pathway. This situation also intrigued us, and therefore, our studies turned to elucidate the role of JMJD6 in the regulation of ferroptosis.

Ferroptosis, a form of iron-dependent and regulated necrosis driven by lipid peroxidation, has demonstrated therapeutic potential in diverse cancer types [30–32]. Thus, to elucidate the role of JMJD6 in ferroptosis, we subjected lung cancer cells with altered JMJD6 expression levels to the ferroptosis inducer erastin, followed by monitoring of specific ferroptosis markers. The results from Reactive oxygen species (ROS) (Fig. 4E) and lipid peroxidation assays (Fig. 4F) indicated that overexpression of JMJD6 led to a reduction in ROS content and malondialdehyde (MDA) levels to a certain degree.

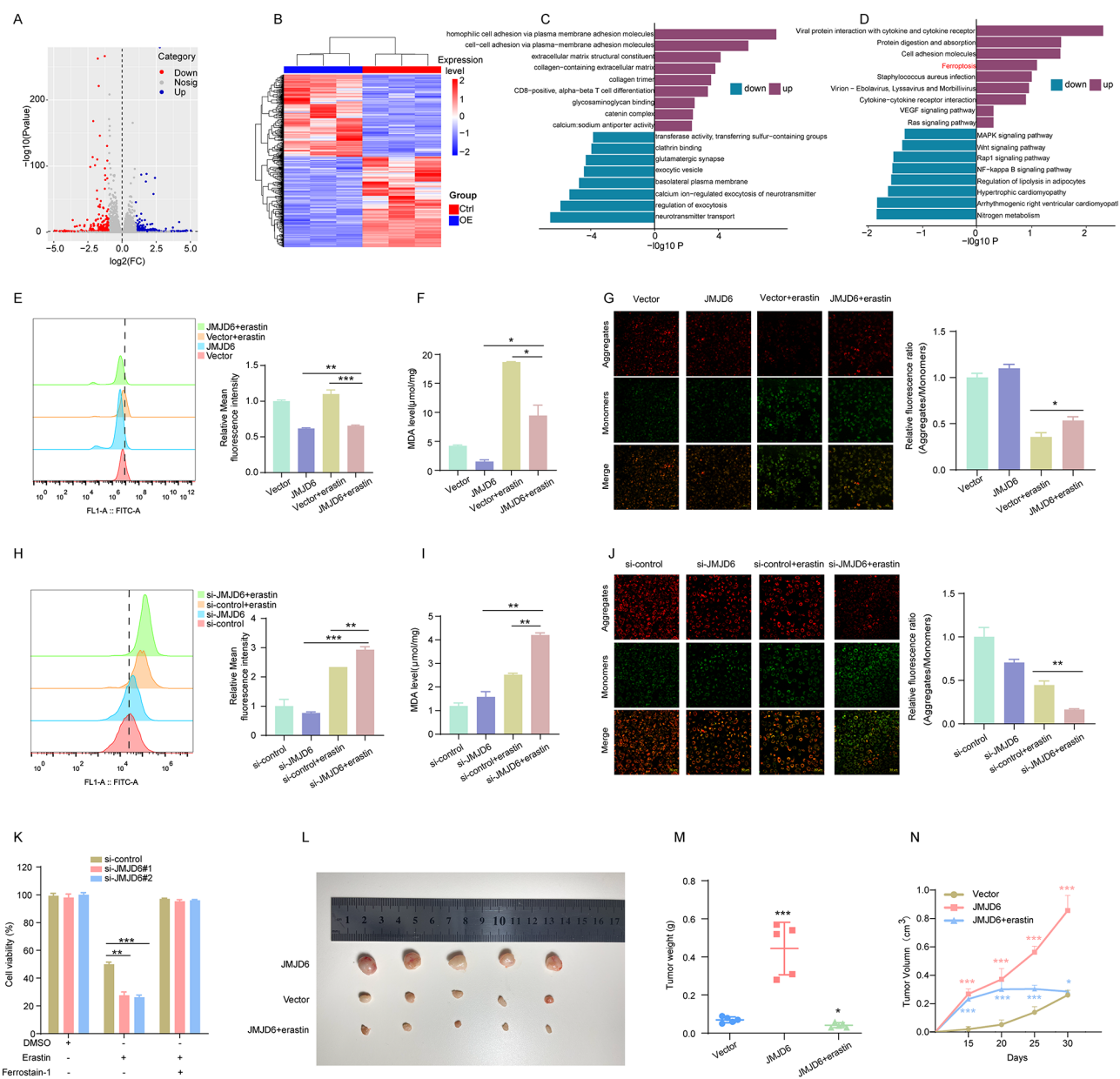


Fig. 4 JMJD6 functions as a negative modulator in regulating lung cancer cell ferroptosis. **(A)** Volcano plot of different gene expression profiles in H1299 cells overexpressing JMJD6. The genes marked in gray were not significantly different, while the genes marked in red and blue showed significant changes in expression levels. **(B)** Heatmap shows the expression ratio of significantly differentially expressed genes (fold change > 1, $P < 0.05$) in RNA-seq analysis. **(C)** Gene Ontology (GO) was used for functional annotation and enrichment analysis of up-regulated and down-regulated genes. Among the up-regulated genes, the top three in BP, CC and MF were selected for enrichment analysis. Among down-regulated genes, the top three enrichment in BP, CC were selected for analysis, while the top two enrichment in MF were selected for analysis. **(D)** The up-regulated and down-regulated Genes were analyzed by Kyoto Encyclopedia of Genes and Genomes (KEGG) pathway. **(E)** Flow cytometry analysis of ROS in JMJD6 overexpression H460 cells. Representative images are shown on the left and statistical data analysis on the right. **(F)** The changes of lipid peroxidation level in JMJD6 over-expressed H1299 cells were detected by MDA method. **(G)** JC-1 fluorescent probe was used to detect the degree of mitochondrial membrane potential depolarization in H1299 cells with JMJD6 overexpression. Representative images are shown on the left and statistical data analysis on the right. The scale bars represent 50 μm . **(H)** ROS content in JMJD6 knockdown H157 cells was detected by flow cytometry. Representative images are shown on the left and statistical data analysis on the right. **(I)** MDA assay was used to detect the changes of lipid peroxidation in JMJD6 knockdown A549 cells. **(J)** JC-1 fluorescent probe was used to detect the changes of mitochondrial membrane potential in JMJD6 knockdown A549 cells. Representative images are shown on the left and statistical data analysis on the right. The scale bars represent 50 μm . **(K)** The JMJD6 knockdown A549 cells were treated with erastin and fer-1, respectively, and the cell viability was detected. **(L, M, N)** Tumor images of nude mice in control group, overexpressed JMJD6 group and overexpressed JMJD6 with injected 30 mg/kg erastin group **(L)**. Tumor weight **(M)** and growth curve **(N)** were measured. Data are presented as mean \pm standard deviation. Data are presented as mean \pm standard deviation. * $p < 0.05$; ** $p < 0.01$; *** $p < 0.001$

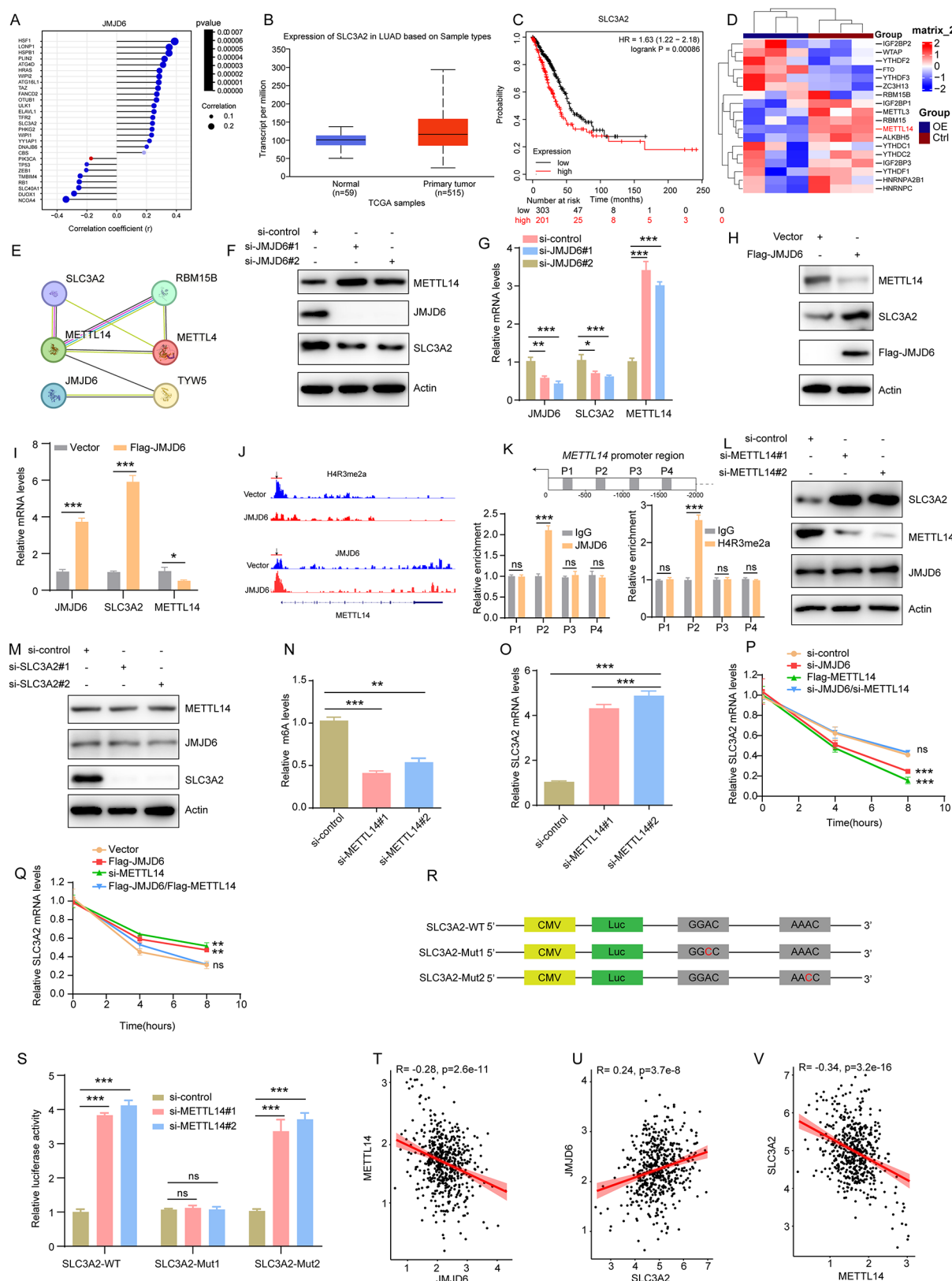


Fig. 5 (See legend on next page.)

(See figure on previous page.)

Fig. 5 JMJD6 inhibits SLC3A2 expression by METTL14 mediated m6A manner. **(A)** The TCGA database was used to analyze the ferroptosis-related genes significantly related to JMJD6 in lung cancer cells. **(B)** TCGA database was used to analyze the expression level of SLC3A2 in lung cancer tissues and normal tissues. **(C)** TCGA data set was used to analyze the Kaplan-Meier survival of lung cancer patients with high SLC3A2 expression. **(D)** Heat map analysis of m6A modification-related enzyme genes was performed. **(E)** Protein-protein interaction network (PPI) was used to analyze the interaction of JMJD6 with METTL14 and SLC3A2. **(F, G)** The expression levels of METTL14 and SLC3A2 in H1299 cells after JMJD6 knockdown were verified by Western blot and RT-qPCR at the protein **(F)** and mRNA **(G)** levels, respectively. **(H, I)** The expression levels of METTL14 and SLC3A2 after JMJD6 overexpression were verified by Western blot and RT-qPCR at the protein level **(H)** and mRNA level **(I)**, respectively. **(J)** CUT&Tag detection, representative trace plots showing the region of JMJD6 binding METTL14 and peak plots regulating changes in its H4R3m2a modification levels. The arrow marks the promoter region. **(K)** ChIP-qPCR was used to verify the binding of JMJD6 and H4R3me2a to the promoter region of METTL14 (500–1000). **(L)** Western blot was used to verify the expression levels of JMJD6 and SLC3A2 after knockdown of METTL14. **(M)** Western blot was used to verify the expression levels of JMJD6 and METTL14 after SLC3A2 knockdown. **(N, O)** METTL14 was knocked down in H1299 cells, and the effect of METTL14 on SLC3A2 expression was verified by detecting the m6A level **(N)** and mRNA expression **(O)** of SLC3A2, respectively. **(P)** The effects of JMJD6 and METTL14 on SLC3A2 expression were verified by detecting the mRNA stability of si-JMJD6 group, METTL14 overexpression group and si-JMJD6/si-METTL14 group. **(Q)** The effects of JMJD6 and METTL14 on SLC3A2 expression were verified by detecting the stability of SLC3A2 mRNA in JMJD6 overexpression group, si-METTL14 group and Flag-JMJD6/Flag-METTL14 group. **(R)** SLC3A2 3'UTR containing either wild-type or mutant (A-to-C mutation) m6A sites was cloned into luciferase reporter vector. **(S)** Relative luciferase activity of the wild-type and mutant form of SLC3A2 3'UTR reporter vectors in A549 cells transfected with si-control or si-METTL14, respectively. **(T, U, V)** The correlation between JMJD6, METTL14 and SLC3A2 was analyzed by TCGA database. Data are presented as mean \pm SD. * $p < 0.05$; ** $p < 0.01$; *** $p < 0.001$

However, following erastin induction, the levels of ROS and MDA in the JMJD6 overexpression group were significantly decreased compared to those in the control group. To further investigate the potential relationship between JMJD6 and ferroptosis, alterations in mitochondrial structure and function were assessed using a JC-1 fluorescent probe to measure the extent of mitochondrial depolarization based on the red to green fluorescence intensity ratio (Fig. 4G and S1A). The findings indicated that upregulation of JMJD6 led to a decrease in mitochondrial depolarization, accompanied an increase in the polymorphism/monomer ratio. Furthermore, the disparity between the control group and the JMJD6 overexpression group was more pronounced following erastin treatment. To validate these results, we silenced JMJD6 expression in lung cancer cells. Treatment with the inducer erastin was then continued, and ROS and MDA content were measured. It was found that JMJD6 knockdown resulted in a certain increase in ROS level (Fig. 4H) and MDA level (Fig. 4I), and attenuated mitochondrial depolarization (Fig. 4J and S1B) compared with the control group, and these differences were exacerbated by the addition of erastin. Cell viability assay showed that the cell viability of A549 cells was significantly decreased after JMJD6 knockdown and erastin addition (Fig. 4K). In order to delve deeper into the impact of JMJD6 on lung cancer progression, in vivo experiments were conducted using a xenograft model. According to (Fig. 4L–N), the tumor volume and weight were notably larger in the group overexpressing JMJD6 compared to the NC group. However, the increase in tumor volume and weight caused by JMJD6 overexpression was significantly attenuated after erastin treatment. Collectively, these results indicate that JMJD6 plays a negative role in regulating lung cancer cell ferroptosis process.

JMJD6 inhibits SLC3A2 expression by METTL14 mediated m6A manner

In order to investigate the precise mechanism by which JMJD6 influences ferroptosis in lung cancer, we examined the relationship between JMJD6 and ferroptosis-related genes by utilizing the TCGA lung cancer database. The results of this analysis showed an association between JMJD6 expression and multiple ferroptosis genes (Fig. 5A). By intersecting these genes with sequencing altered genes, we identified that SLC3A2 is not only correlated with JMJD6 expression, but also undergoes alteration with JMJD6 overexpression. Therefore, we focused on SLC3A2 to investigate its potential role in mediating JMJD6 regulation of ferroptosis in lung cancer cells. Then, we analyzed the association between SLC3A2 and lung cancer, and found elevated expression of SLC3A2 in cancerous tumor tissues compared to normal tissues (Fig. 5B). Additionally, lower overall survival rates were observed in cases with higher SLC3A2 expression (Fig. 5C). Previous studies have indicated that RNA m6A modification can impact the regulation of ferroptosis genes [33, 34]. To clarify whether JMJD6 can also regulate the expression of SLC3A2 by affecting m6A modification, we reanalyzed the changes in m6A modified regulatory genes in the sequencing data. Multiple m6A modified regulatory genes exhibited alterations, with METTL14 demonstrating the highest frequency of changes (Fig. 5D). And we again verified the interaction between JMJD6 and METTL14 by protein interaction analysis (PPI) (Fig. 5E). Subsequently, RT-qPCR and Western blot experiments confirmed that METTL14 was significantly up-regulated after JMJD6 knockdown, while SLC3A2 was significantly down-regulated at both mRNA and protein levels (Fig. 5F and G). After JMJD6 overexpression, METTL14 expression was significantly down-regulated at both mRNA and protein levels, while SLC3A2 expression was significantly up-regulated at both mRNA and protein levels (Fig. 5H and I).

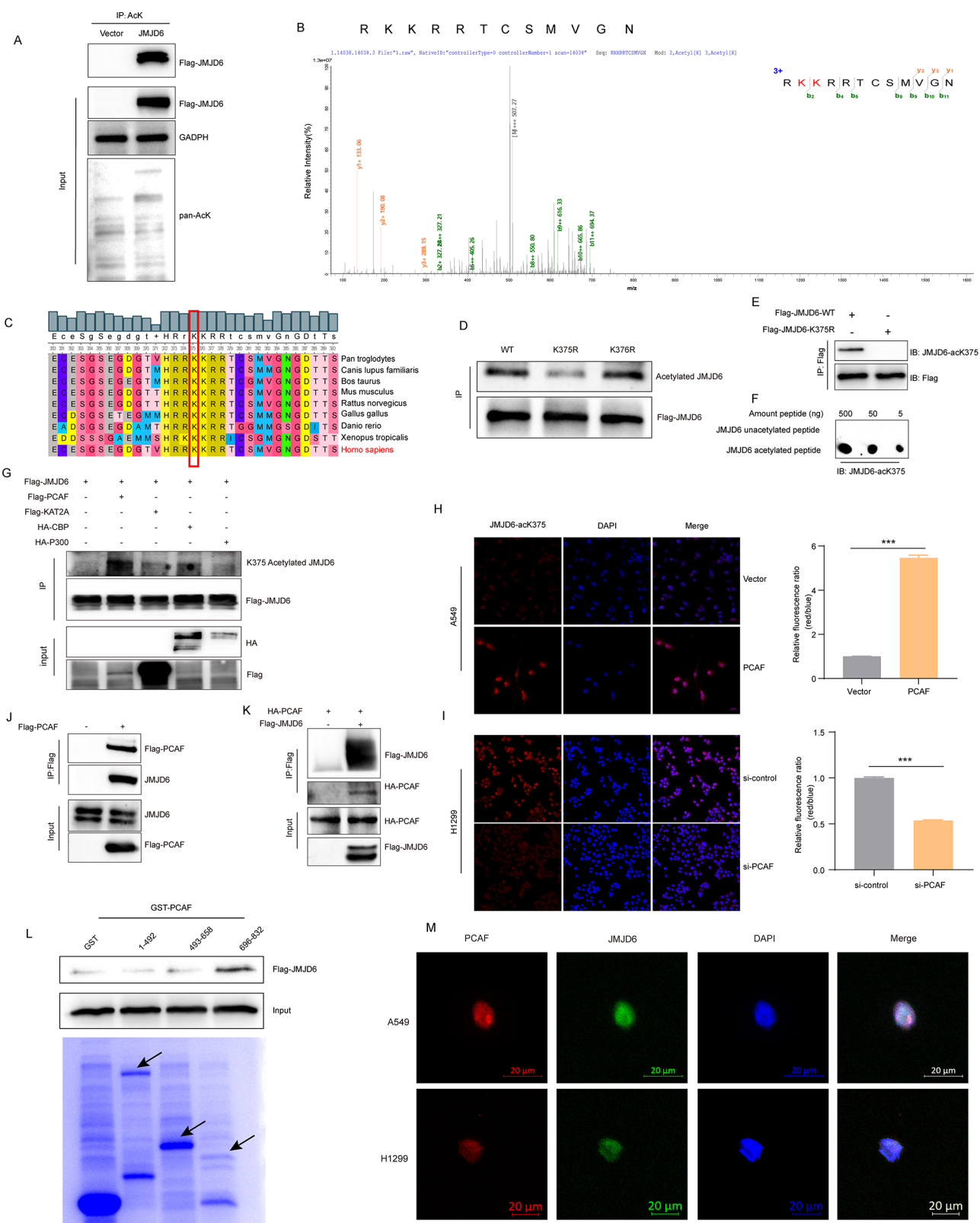
To elucidate the precise interaction mechanism among JMJD6, METTL14, and SLC3A2, we undertook a comprehensive investigation. JMJD6 is known to have histone arginine demethylase activity, removing methyl groups from either symmetric (H4R3me2s) or asymmetric (H4R3me2a) methylated arginine, and H4R3me2a is an important marker for transcriptionally active chromatin [35, 36]. Therefore, to investigate whether JMJD6 regulates METTL14 expression through its arginine demethylase activity, we first examined the enrichment of JMJD6 on the METTL14 genome and the modification of METTL14 using CUT&Tag technology in the control and JMJD6 overexpression groups (Fig. 5J). The results showed that JMJD6 overexpression significantly increased its enrichment level in the promoter region of METTL14 gene compared with the control group. H4R3me2a modification was also mainly distributed in the promoter region of METTL14, and the overexpression of JMJD6 significantly reduced the abundance of H4R3me2a in the promoter region. Subsequently, to determine the exact binding site of JMJD6 regulating METTL14 H4R3me2a demethylation, we performed ChIP-qPCR and found that both JMJD6 and H4R3me2a bind to the METTL14 promoter (500–1000). This promoter is located upstream of the METTL14 transcription start site (TSS) (Fig. 5K). Furthermore, we found that the upregulation of SLC3A2 was observed following the depletion of METTL14, whereas the expression of JMJD6 remained relatively unchanged (Fig. 5L). Conversely, the knockdown of SLC3A2 did not result in significant alterations in the expression levels of JMJD6 and METTL14 (Fig. 5M), indicating that SLC3A2 does not play a significant role in regulating the expression of JMJD6 and METTL14.

METTL14, a member of the m6A methylation modifying enzyme family, is involved in the regulation of RNA m6A modification. Therefore, we hypothesized that METTL14 may influence SLC3A2 expression by altering the m6A modification level of SLC3A2 mRNA. Interestingly, MeRIP assay showed that the m6A level of SLC3A2 mRNA was significantly reduced after knockdown of METTL14 (Fig. 5N), while RT-qPCR results indicated a significant increase in the expression level of SLC3A2 mRNA following METTL14 knockdown (Fig. 5O). Then, we also examined the changes in SLC3A2 mRNA stability under different treatment conditions using the transcription inhibitor Actinomycin D. The findings indicated that JMJD6 knockdown had the same inhibitory effect on SLC3A2 mRNA stability as METTL14 overexpression, but the inhibitory effect caused by JMJD6 knockdown was significantly relieved after METTL14 knockdown (Fig. 5P and S4A). On the contrary, overexpression of JMJD6 had the same effect as knockdown of METTL14, both of which promoted the stability of SLC3A2 mRNA,

and the promotion effect brought by overexpression of JMJD6 was significantly relieved after overexpression of METTL14 (Fig. 5Q and S4B). In addition, to further verify the effect of m6A modification of SLC3A2 on its mRNA stability. We also performed a dual luciferase reporter assay. SRAMP software was used to predict the m6A modification sites of SLC3A2 mRNA. Based on the predicted results, two of the putative m6A sites were mutated (A to C) to construct wild-type SLC3A2 (3'UTR-WT) and mutant SLC3A2 (3'UTR-Mut1 and 3'UTR-Mut2) luciferase reporter plasmids (Fig. 5R), and the luciferase activity of the wild-type or mutant SLC3A2-fused reporter was measured in control and METTL14-knockdown H1299 and A549 cells. The results showed that METTL14 knockdown improved mRNA stability (firefly luciferase activity as a proxy for mRNA stability) in both the SLC3A2-WT and SLC3A2-Mut2 groups, whereas this increase was not observed when the SLC3A2-Mut1 reporter was introduced (Fig. 5S and S4C). Again, this indicates that SLC3A2 downregulation is mediated by METTL14-mediated m6A modification, which reduces SLC3A2 mRNA stability. Subsequently, we performed correlation analysis of the expression levels of JMJD6, METTL14 and SLC3A2 in TCGA lung cancer database, and found that JMJD6 was negatively correlated with METTL14 (Fig. 5T), positively correlated with SLC3A2 (Fig. 5U), and METTL14 was negatively correlated with SLC3A2 (Fig. 5V). These results suggest that JMJD6 affects METTL14 expression in an arginine demethylase dependent manner, thereby mediating m6A modification of SLC3A2 to regulate its expression level.

JMJD6 is acetylated at lysine 375 by PCAF

There are few reports about how JMJD6 was regulated, and there was no report about the protein post-translational modifications (PTM) in JMJD6. In an attempt to identify JMJD6 PTM, we found that JMJD6 is an acetylated protein in living cells. Specifically, we utilized anti-acetylated lysine antibody immunoprecipitation in lung cancer cells and checked whether JMJD6 protein can be detected in the pull-down samples. Intriguingly, JMJD6 was identified as an acetylated protein within the co-immunoprecipitation complex (Fig. 6A). The possible acetylation sites of JMJD6 were identified by liquid chromatography-mass spectrometry and Lysins 375 and 376 were found to be acetylated and conserved in multiple species (Fig. 6B and C). Therefore, we used pan-acetylation antibody to verify the acetylation of JMJD6 with K375 and K376 gene mutations, and the results showed that only the deletion mutation of lysine 375 (K375R) could reduce the acetylation level, confirming that lysine 375 is a major acetylation modification site of JMJD6 (Fig. 6D). So, we synthesized a K375 site specific acetylation antibody based on this, and verified its



(See figure on previous page.)

Fig. 6 JMJD6 is acetylated at lysine 375 by PCAF. **(A)** Flag tagged JMJD6 expression vector was introduced into H1299 cells and cell lysates were then immunoprecipitated with anti-acetylated lysine (AcK) antibody or normal IgG followed by immunoblotting with anti-Flag antibody. **(B)** Liquid chromatography-mass spectrometry (LC/MS) was used to detect the lysine site of JMJD6, and the spectrum displayed the acetylation sites of JMJD6. **(C)** The sequences adjacent to human JMJD6-K375 from different JMJD6 homologues species were aligned. **(D)** Flag-tagged JMJD6-WT, JMJD6-K375R and JMJD6-K376R mutants were co-transfected with PCAF into H1299, respectively. Cell lysates were co-precipitated with anti-Flag antibody and immunoblotted with pan-acetylated antibody. **(E, F)** Western blot and dot blot hybridization assays were used to detect the efficiency of JMJD6-acK375-specific acetylation antibody. **(G)** Flag-JMJD6 expression vector and multiple acetyltransferase expression vectors were co-transfected into H1299 cells, and Western blot analysis was performed with JMJD6-acK375 antibody to explore the acetylase of JMJD6. **(H)** site-specific acetylation of K375 by JMJD6 was detected by immunofluorescence in PCAF overexpressing A549 cells. Scale bars represent 20 μ m. **(I)** site-specific acetylation of K375 by JMJD6 was detected by immunofluorescence in PCAF knockdown H1299 cells. Scale bars represent 50 μ m. **(J)** Flag-PCAF expression vector was transfected into H1299 cells, and the interaction between JMJD6 and PCAF was detected by Western blot. **(K)** HA-PCAF and Flag-JMJD6 expression vectors were introduced into H1299 cells and co-immunoprecipitated with Flag gel beads followed by detection with the labeled antibodies. **(L)** The lysates of Flag-JMJD6 transfected H1299 cells were used for GST pull-down assay. Western blot was performed with anti-Flag and the purified GST-PCAF fusion protein was detected by Coomassie brilliant blue staining. Arrows indicate the correct molecular weight of the corresponding protein. **(M)** Laser confocal microscopy was used to detect the co-localization of PCAF (red) and JMJD6 (green). Nuclei were stained with DAPI (blue). Scale bars represent 20 μ m. Data are expressed as mean \pm SD. * $p < 0.05$; ** $p < 0.01$; *** $p < 0.001$

specificity by Western blot (Fig. 6E) and dot blot (Fig. 6F). Additionally, acetylation of JMJD6 was observed upon ectopic expression of acetyltransferase PCAF, while other acetyltransferases such as CBP, p300, and KAT2A did not exhibit this effect (Fig. 6G). Subsequently, the acetylation of PCAF on the JMJD6 K375 site was confirmed through immunofluorescence staining. A549 and H1299 cells were subjected to overexpression and knockdown of PCAF, followed by incubation with the antibody specific to the JMJD6-acK375 site. Knockdown of PCAF resulted in a reduction of JMJD6 acetylation at K375 (Fig. 6I and S2A), while overexpression of PCAF led to an increase in the acetylation level of JMJD6 (Fig. 6H and S2B). Thus, we pinpointed for the first time that JMJD6 is able to be acetylated by PCAF, representing a paradigm that JMJD6 can be post-translationally modified.

Given that PCAF acetylated JMJD6, we speculate that there may be a direct interaction between them. Endogenous JMJD6 was immunoprecipitated by Flag tagged PCAF in H1299 cells (Fig. 6J). In addition, exogenously expressed JMJD6 and PCAF could be immunoprecipitated using different tag antibodies (Fig. 6K). These findings unequivocally establish the presence of both endogenous and exogenous interactions between JMJD6 and PCAF in living cells. In order to ascertain the specific binding region of JMJD6 to PCAF, three GST fusion proteins encompassing the N-terminal, HAT, and Bromo domains of PCAF were initially generated and produced from *E. coli* BL21. Subsequent GST pull-down analysis revealed that JMJD6 predominantly associates with the Bromo domain of PCAF (Fig. 6L). Furthermore, immunofluorescence staining demonstrated the co-localization of JMJD6 and PCAF within the nucleus (Fig. 6M and S2C). Consequently, these findings indicate that JMJD6 has the capacity to interact with PCAF in both in vitro and in vivo.

JMJD6 acetylation inhibits NSCLC progression and xenograft growth by promoting ferroptosis

In order to investigate the impact of JMJD6 K375 acetylation on the proliferation, migration, and invasion capabilities of lung cancer cells, we established stable overexpression of JMJD6 WT, K375R and JMJD6 K375Q cell line (Fig. 7A). It needs to be explained that in general, mutation of lysine (K) to arginine (R) is equivalent to simulated deacetylation, and mutation of lysine to glutamine (Q) is equivalent to simulated acetylation. Through the utilization of CCK-8 (Fig. 7B), EdU (Fig. 7C and S3A), and colony formation assays (Fig. 7D) to assess cell proliferation, it was observed that the JMJD6 K375R mutant exhibited a significantly heightened cell proliferation capacity compared to wild-type cells, whereas the acetylated mutant JMJD6 K375Q demonstrated a notable decrease in cell proliferation ability. Next, transwell assays indicated that cells expressing JMJD6-K375R exhibited a notable enhancement in migration and invasion capabilities compared to JMJD6-WT, whereas JMJD6-K375Q group demonstrated a significant reduction (Fig. 7E). Besides, as shown in Fig. 7F, xenograft tumors in mice expressing JMJD6-K375R exhibited notably accelerated tumor growth and increased tumor volume in comparison to those expressing JMJD6-WT. Conversely, JMJD6-K375Q displayed a decelerated tumor growth rate and reduced tumor volume compared to tumor expressing JMJD6-WT (Fig. 7F-H). These findings collectively support the conclusion that acetylation of JMJD6 K375 acetylation suppresses the proliferation, migration, and invasion of lung cancer cells, as well as inhibiting xenograft tumor growth in mice.

Considering JMJD6 regulates ferroptosis in lung cancer cells, we are interested in testing whether acetylation will affect its regulation of ferroptosis, thereby influencing lung cancer development. Interestingly, there were no significant differences in ROS levels (Fig. 7I), and cell viability (Fig. 7J) among H1299 cells expressing JMJD6-WT, JMJD6-K375R, and JMJD6-K375Q. However, after

erastin treatment, the ROS level of JMJD6-K375R group (Fig. 7I) was significantly lower than that of JMJD6-WT group, while the cell viability of JMJD6-K375R group (Fig. 7J) was significantly higher than that of JMJD6-WT group. The opposite was observed in JMJD6-K375Q group. Treatment with the ferroptosis inhibitor Ferrostatin-1 (Fer-1) markedly attenuated this difference. Additionally, following erastin treatment, the degree of mitochondrial depolarization was significantly lower in the JMJD6-K375R group compared to the JMJD6-WT group, whereas the JMJD6-K375Q group exhibited a significant increase in mitochondrial depolarization (Fig. 7K and S3B). In addition, immunohistochemical results showed that the expressions of SLC3A2, GPX4, XCT and Ki67, which were negatively correlated with ferroptosis, were significantly increased in the JMJD6-K375R group compared with the wild type control group, while the expressions of these indexes were significantly decreased in the JMJD6-K375Q group compared with the wild type control group (Fig. 7L). These results suggest that acetylation of JMJD6 K375 may hinder the progression of lung cancer by enhancing the regulation of ferroptosis in lung cancer cells.

Acetylation weakens the activity of JMJD6 in regulating METTL14 expression and affecting its mediated m6A modification to regulate SLC3A2

To investigate the molecular mechanism by which JMJD6 acetylation affects the regulation of ferroptosis, we first investigated the effect of acetylation modification on the JMJD6/METTL14/SLC3A2 signaling axis. The effect of acetylation at K375 of JMJD6 on METTL14 expression was examined by western blot and RT-qPCR, respectively. Interestingly, we observed a significant reduction in METTL14 expression in the acetylation deficient mutant group and a significant increase in the expression of METTL14 in JMJD6-K375Q compared to JMJD6-WT (Fig. 8A and B). Notably, JMJD6 had no effect on its expression before and after acetylation modification at K375, so we hypothesized that JMJD6 acetylation may affect the downstream expression of METTL14 by regulating its demethylase activity. Subsequently, we used H4R3me2a antibody to perform METTL14 enrichment analysis in cells with different JMJD6 acetylation modification states to explore whether acetylation of JMJD6 K375 would alter the H4R3me2a level of METTL14. Our findings showed that the enrichment level of H4R3me2a in METTL14 was significantly lower in the JMJD6-K375R group and significantly higher in the JMJD6-K375Q group compared with the JMJD6-WT group (Fig. 8C). These results suggest that acetylation of JMJD6 K375 attenuated demethylation of the METTL14 promoter region, resulting in increased H4R3me2a levels and ultimately increased METTL14 expression.

Besides, there was a notable increase in the expression of SLC3A2 in JMJD6-K375R, whereas a significant decrease was observed in the expression of SLC3A2 in JMJD6-K375Q compared to JMJD6-WT (Fig. 8D and E). And it's worth noting, the m6A level of SLC3A2 was also impacted, with the m6A level in the JMJD6-K375Q group showing a significant increase and a decrease in the JMJD6-K375R group relative to the JMJD6-WT group (Fig. 8F). To verify that the regulation of m6A modification level on SLC3A2 mRNA by acetylated JMJD6 was still dependent on METTL14, the change of m6A level in SLC3A2 after knockdown of METTL14 was verified in JMJD6-WT and JMJD6-K375R groups. The results showed that there was no significant difference in the m6A level of SLC3A2 between JMJD6-WT and JMJD6-K375R in the METTL14 knockdown group (Fig. 8G). Similarly, we repeated the experimental manipulations in the JMJD6-WT and JMJD6-K375Q groups and also obtained consistent experimental results (Fig. S4D). These results suggest that acetylated JMJD6 modulates the m6A levels of SLC3A2 by regulating METTL14. Subsequently, it influences the regulation of SLC3A2 expression. To verify that the regulation of ferroptosis by acetylated JMJD6 at K375 is dependent on SLC3A2 expression, several reversion assays were designed. The first is the cell proliferation assay (Fig. 8H). In line with prior findings, cell proliferation was notably elevated in the JMJD6-K375R group compared to the WT group. Nevertheless, no significant disparity in cell proliferation was observed between the JMJD6-K375R group and the WT group following SLC3A2 knockdown. We also verified the differences in cell viability (Fig. 8I) and ROS levels (Fig. 8J), and found that there was no significant difference between the two groups before erastin treatment. Subsequent to treatment, the cell viability of the JMJD6-K375R group exhibited a notable increase compared to the WT group, while the ROS content was significantly lower. Notably, SLC3A2 knockdown in both the JMJD6-K375R and WT groups did not result in significant alterations in cell viability or ROS content. These findings further confirm that acetylation of the JMJD6 K375 site attenuates the demethylase activity of its H4R3me2a, which enhances the expression of METTL14, affects its mediated m6A modification of SLC3A2, and ultimately promotes the iron death response in lung cancer cells.

Elevated JMJD6 acetylation predicts a favorable survival in NSCLC patients

Given that the acetylated defective JMJD6-K375R mutant promotes lung cancer cell migration and tumor growth in mice, it will be interesting to know whether JMJD6-K375 acetylation is present to varying degrees in lung cancer patients. To this end, we used anti-JMJD6-acK375 antibody to detect the acetylation level of JMJD6 in 68

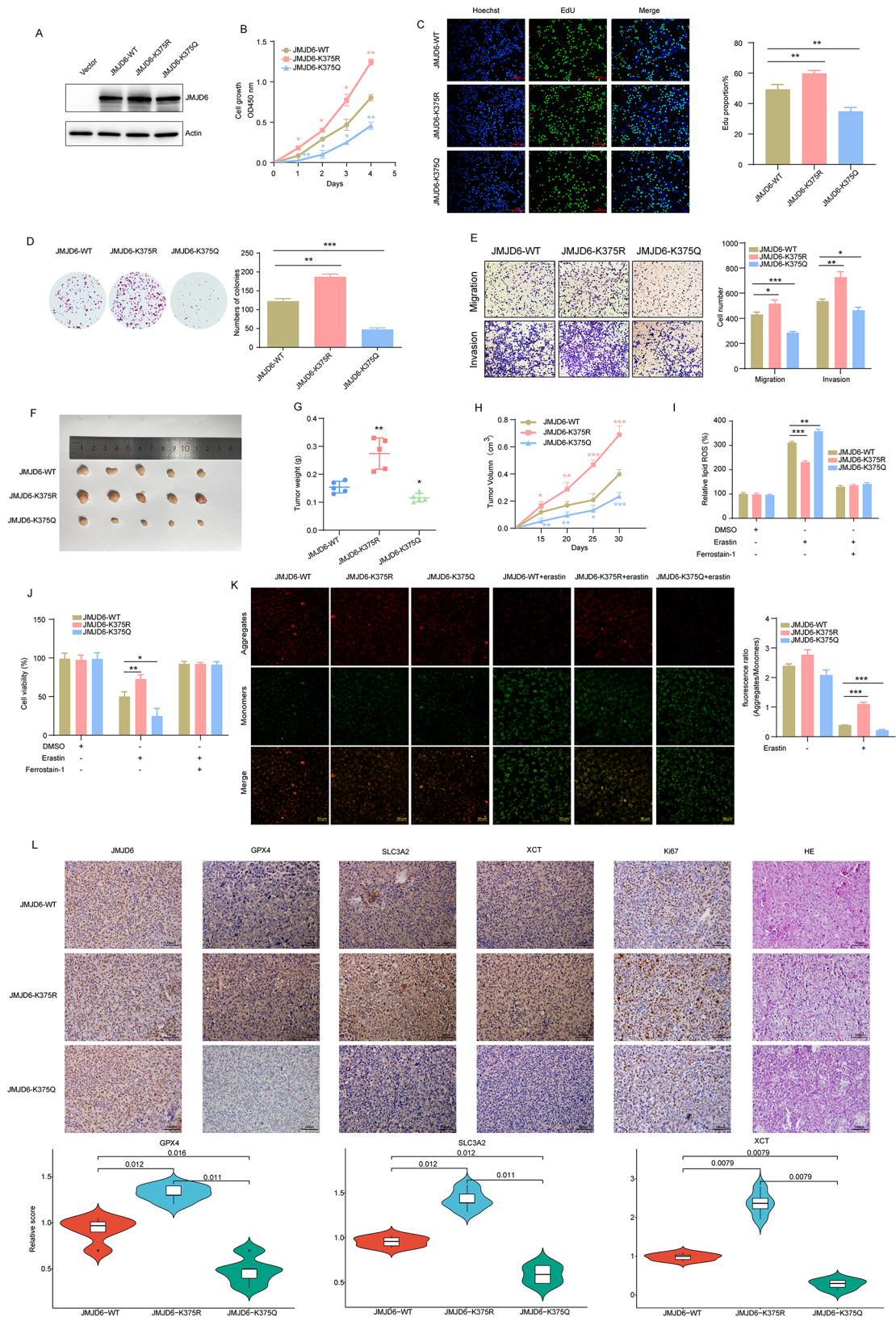


Fig. 7 (See legend on next page.)

(See figure on previous page.)

Fig. 7 JMJD6 acetylation inhibits NSCLC progression and xenograft growth by promoting ferroptosis. **(A)** H1299 cells stably expressing JMJD6-WT, JMJD6-K375R and JMJD6-K375Q were established, and the expression of target proteins was confirmed by Western blot analysis with JMJD6 antibody. **(B)** CCK-8 was used to detect the effect of JMJD6-K375 acetylation on the proliferation of H1299 cells. **(C)** EdU was used to detect the effect of JMJD6-K375 acetylation on the proliferation of H1299 cells. Representative images are shown on the left and statistical data analysis on the right. The scale bars represent 100 μ m. **(D)** Colony formation assay was used to detect the effect of JMJD6-K375 acetylation on the proliferation of H1299 cells. Representative pictures are shown on the left and statistical data analysis on the right. **(E)** Transwell assay was used to detect the effect of JMJD6-K375 acetylation on the migration and invasion of H1299 cells. Representative pictures are shown on the left and statistical data analysis on the right. **(F, G, H)** Mice were injected with H1299 cells expressing JMJD6-WT, JMJD6-K375R and JMJD6-K375Q. **(H)** The growth curve of transplanted tumor in nude mice was drawn. **(F, G)** On the 30th day, the images of transplanted tumors were dissected and taken, and the average tumor weight was measured. **(I)** The effect of JMJD6 acetylation on ROS level in NSCLC cells. **(J)** JMJD6 acetylated NSCLC cells were treated with erastin and ferrostatin-1, and cell viability was detected. **(K)** JC-1 fluorescent probe was used to detect the change of mitochondrial membrane potential in H1299 cells after acetylation of JMJD6. Representative pictures are shown on the left and statistical data analysis on the right. The scale bars represent 50 μ m. **(L)** Expression of JMJD6, GPX4, SLC3A2, xCT and Ki67 in serial sections of subcutaneous xenograft tumors. Representative images are shown at the top and statistical data analysis is shown at the bottom. The scale bars represent 100 μ m. Data are expressed as mean \pm SD. * p < 0.05; ** p < 0.01; *** p < 0.001

lung cancer patients by immunohistochemical method, and found that JMJD6 acetylation level was higher in the adjacent tissues (Fig. 9A). Next, the relationship between JMJD6 acetylation expression and the clinical pathological characteristics of lung cancer patients were investigated. The results indicated a positive correlation between elevated levels of JMJD6 acetylation and smaller tumor size as well as lower clinical stage in lung cancer cases (Fig. 9B). Statistical analysis further demonstrated that the expression of JMJD6-acK375 was significantly higher in stage I-II compared to stages III-IV (Fig. 9C), and its expression was also higher in tumor tissues < 5 cm than \geq 5 cm (Fig. 9D). Moreover, we also found that JMJD6 acetylation level was significantly associated with the prognosis of lung cancer patients, and patients with elevated JMJD6-K375 acetylation level had better overall survival than those with low acetylation level (Fig. 9E). Therefore, these results suggest that elevated JMJD6 acetylation predicts a favorable survival in NSCLC patients.

Discussion

Lung cancer is one of the most common malignant tumors in the world, with high morbidity and mortality [37]. Despite a decline in both incidence and mortality rates in recent years, lung cancer remains the second most frequently diagnosed cancer globally. Lung cancer can be classified into two main pathological subtypes: non-small cell lung cancer (NSCLC) and small cell lung cancer (SCLC). NSCLC, comprising 85–90% of all lung cancer cases, is typically diagnosed at an advanced stage, leading to a dismal prognosis. Currently, various treatment modalities including surgery, radiotherapy, chemotherapy, immunotherapy, and molecular targeted therapy are utilized for the management of NSCLC. In recent years, small molecule tyrosine kinase inhibitors (TKIs) have emerged as a promising therapeutic option for NSCLC, demonstrating efficacy in treatment [38]. Despite these advancements, challenges such as distant metastasis, drug resistance, and local recurrence persist, leading to suboptimal treatment outcomes for a subset of patients [7, 8]. Hence, it is imperative to further

investigate additional molecular pathways underlying the pathogenesis and progression of NSCLC and devise appropriate therapeutic strategies. The present study introduces a theoretical framework in which JMJD6 acetylation modulates ferroptosis in lung cancer cells through its influence on the expression of the ferroptosis-associated protein SLC3A2 in a METTL14-dependent fashion.

Jumonji domain-containing 6 (JMJD6), a member of the Jumonji (JMJC) domain family of histone demethylases, relies on Fe^{2+} and α -ketoglutarate for its enzymatic function [39, 40]. The demethylation activity of JMJD6 plays a role in transcriptional regulation, epigenetics, and other biological processes [10]. JMJD6 has been implicated in various tumor regulation as a demethylase. It has been demonstrated that JMJD6, which is highly expressed in breast cancer, interacts with the p19ARF promoter to inhibit Myc-induced apoptosis in various stress conditions by demethylating H4R3me2a [41]. Additionally, JMJD6 plays a role in regulating the invasiveness of glioblastoma through its involvement in epigenetic histone demethylation [42]. In castration-resistant prostate cancer (CRPC), JMJD6 is implicated in demethylating histone H3R or H4R at the androgen receptor (AR) promoter, leading to increased AR mRNA transcription via its demethylase activity and interaction with U2AF65 [43]. However, the molecular regulatory mechanism for JMJD6 regulation in lung cancer remains largely unclear. This study observed elevated levels of JMJD6 expression in tumor tissue compared to normal tissue, with a positive correlation between high JMJD6 expression and advanced clinical stage in lung cancer. Patients with high JMJD6 expression exhibited a poorer prognosis compared to those with low expression levels. The demethylation activity of JMJD6 was reconfirmed in lung cancer cells, demonstrating its ability to modulate histone demethylation of METTL14 and subsequently regulate ferroptosis pathways. Thus, JMJD6 tends to act as a tumor promoter in lung cancer progression by regulating cancer cell proliferation and migration.

Ferroptosis, a recently discovered form of cell death, is characterized by iron-dependent lipid peroxidation

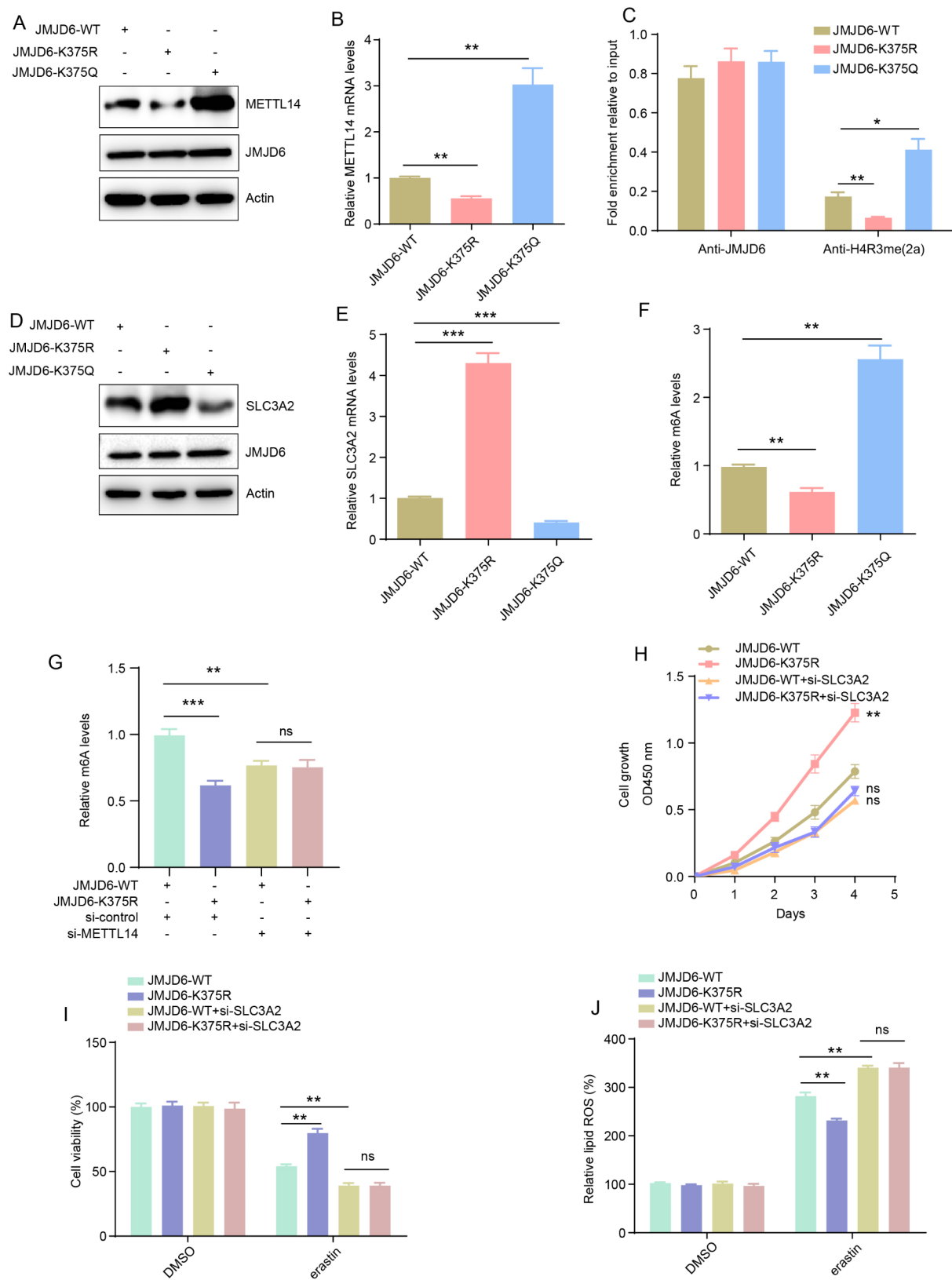


Fig. 8 (See legend on next page.)

(See figure on previous page.)

Fig. 8 Acetylation weakens the activity of JMJD6 in regulating METTL14 expression and affecting its mediated m6A modification to regulate SLC3A2. **(A, B)** Western blot **(A)** and RT-qPCR **(B)** were used to detect the effect of JMJD6 acetylation on METTL14 expression at the protein and mRNA levels, respectively. **(C)** CHIP assay was used to verify the regulation of JMJD6 acetylation on the enrichment level of H4R3me2a in the promoter region of METTL14. **(D, E)** Western blot **(D)** and RT-qPCR **(E)** were used to detect the effect of JMJD6 acetylation on SLC3A2 expression at the protein and mRNA levels, respectively. **(F)** MeRIP was used to detect the m6A level of SLC3A2 in JMJD6-WT, JMJD6-K375R and JMJD6-K375Q groups, and to verify the effect of JMJD6 acetylation on the m6A modification level of SLC3A2 mRNA. **(G)** MeRIP was used to detect the effect of METTL14 knockdown and JMJD6 mimics K375 deacetylation on the m6A modification of SLC3A2 mRNA. **(H)** CCK-8 was used to detect the effect of SLC3A2 knockdown and JMJD6 acetylation deletion on cell proliferation. **(I, J)** Cell viability **(I)** and ROS levels **(J)** were detected in H1299 cells to assess whether SLC3A2 knockdown would alter the sensitivity to erastin. Data are expressed as mean \pm SD. * $p < 0.05$; ** $p < 0.01$; *** $p < 0.001$

and high levels of reactive oxygen species. An increasing number of studies indicate that the ferroptosis process of tumor cells is regulated by m6A modification. It has been reported the m6A reader YT521-B homolog 2 (YTHDC2) indirectly hinders the expression of Homeobox A13 (HOXA13) and SLC3A2 in lung cancer cells by recognizing m6A modification, thereby promoting ferroptosis [44]. Moreover, another m6A reader, insulin-like growth factor 2 mRNA binding protein 3 (IGF2BP3), has been identified as highly expressed in lung cancer cells, playing a role in maintaining the expression levels and mRNA stability of various ferroptotic factors, including SLC3A2, through recognition of m6A modification in their target genes. This mechanism ultimately serves to suppress ferroptosis in lung cancer cells [45]. This suggests that SLC3A2 plays a crucial role in the progression of cancer through ferroptosis, but the specific upstream and downstream pathways and mechanisms involving SLC3A2 are not well elucidated. Although research has shown a correlation between METTL14 and SLC3A2 in colon cancer cells [34], the regulatory connection between these two proteins in lung cancer cells remains unexplored. In this study, we started from the discovery of the new upstream target JMJD6 and refined the downstream regulation pathway and mechanism of ferroptosis. We found that JMJD6 could regulate the H4R3me2a level in the METTL14 promoter region to affect the expression of METTL14, and METTL14 could affect the expression of SLC3A2 by regulating the mRNA m6A level of SLC3A2, thereby affecting the ferroptosis process of NSCLC.

Acetylation is catalyzed by acetyltransferase (KAT), which transfers acetyl groups from acetyl-CoA to the ϵ -amino side chain of lysine [46]. It has been demonstrated that acetylation plays a crucial role in various physiological processes, such as transcriptional and metabolic regulation. Dysregulation of lysine acetylation in specific proteins has been implicated in the pathogenesis of numerous serious diseases, including cancer. The activation of H3K27 acetylation in the STRIP2 promoter region by P300/CBP leads to the transcription of STRIP2 in NSCLC. This transcriptional activation of STRIP2 then influences the stability of TMBIM6 mRNA in an m6A-dependent manner through its interaction with IGF2BP3, ultimately contributing to the progression of NSCLC

[47]. Furthermore, the acetyltransferase GCN5 has been shown to enhance the migration and invasion of NSCLC by facilitating the acetylation of lysine 118 of the SOX4 gene and upregulating the expression of the MMP9 gene [48]. Our previous studies have demonstrated that PCAF has the capability to interact with HOXB9 and acetylate its lysine 27 in both in vivo and in vitro settings. This acetylation of HOXB9 has been found to impede the progression of lung adenocarcinoma by directly suppressing the transcription of its target gene JMJD6 through activation of its promoter [49]. Inspired by these studies, our current study aims to explore the acetylation of JMJD6, its potential interacting acetylase, and the mechanisms underlying their interaction. Our study revealed that JMJD6 protein undergoes acetylation by PCAF in vivo, leading to an increase in H4R3me2a levels in the METTL14 promoter region and subsequent upregulation of METTL14 expression. Elevated METTL14 expression, in turn, results in increased m6A modification of SLC3A2 mRNA and subsequent downregulation of SLC3A2 expression.

In summary, we elucidated the mechanistic underpinnings of the JMJD6-induced ferroptosis phenotype in lung cancer, identifying the PCAF-JMJD6-METTL14-SLC3A2 axis as a key mediator of this cellular process. Our findings unveil a novel signaling pathway by which PCAF facilitates the acetylation of JMJD6 at K375, leading to the modulation of downstream METTL14 and SLC3A2 expression and ultimately suppressing ferroptosis. Nevertheless, further investigation is needed to comprehensively elucidate the role of JMJD6 acetylation in the regulation of ferroptosis mediated by SLC3A2. Therefore, this study has identified a potential therapeutic approach for lung cancer, and JMJD6 may serve as a potentially prognostic biomarker and therapeutic target in the treatment of lung cancer in the future.

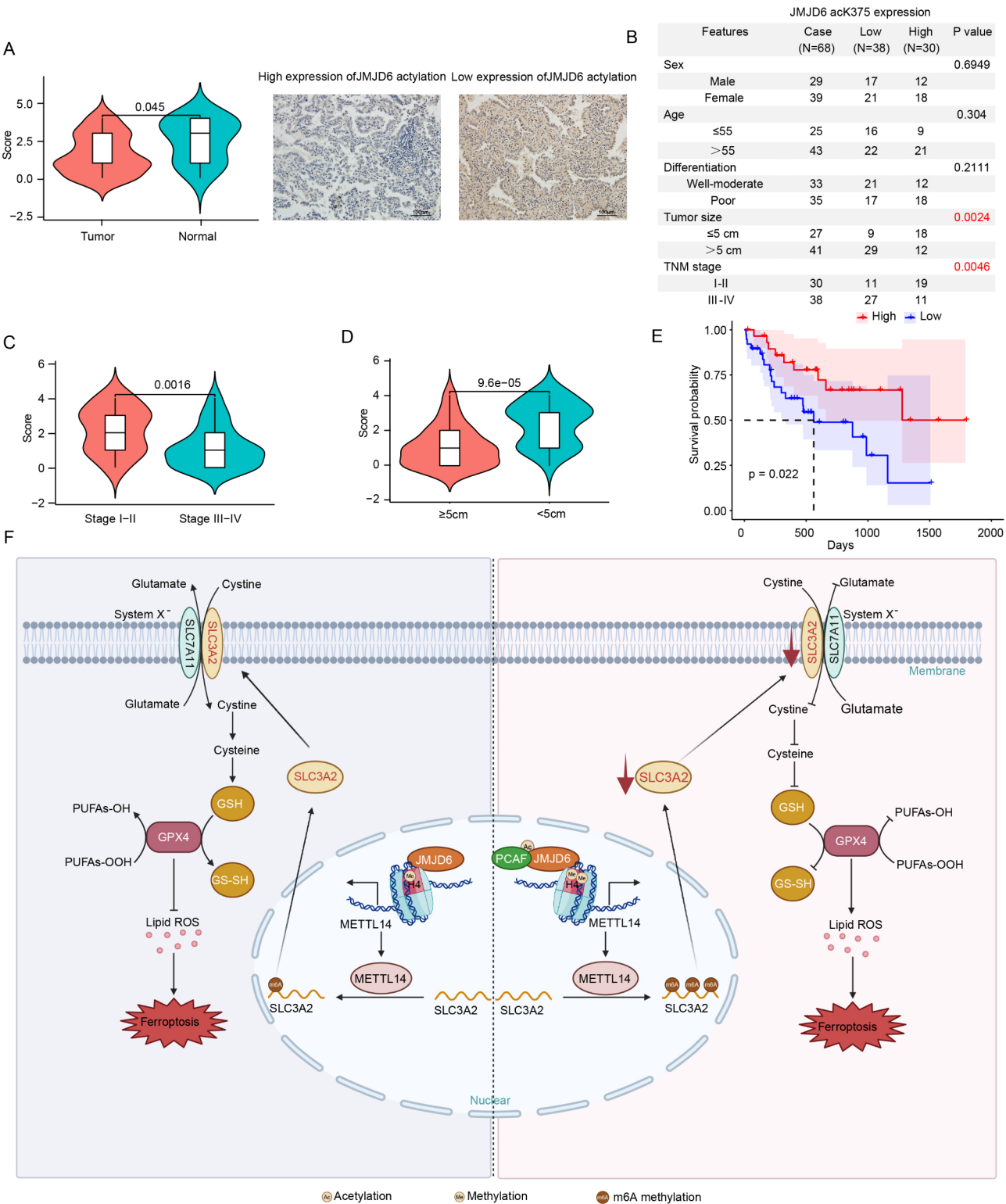


Fig. 9 (See legend on next page.)

(See figure on previous page.)

Fig. 9 Elevated JMJD6 acetylation predicts a favorable survival in NSCLC patients. **(A)** The acetylation level of JMJD6 was detected by immunohistochemistry in 68 cases of lung cancer and precancerous lesions. Representative images are shown on the right and statistical data analysis on the left. The scale bars represent 100 μ m. **(B)** Sixty-eight lung cancer patients were clinically selected and divided into two groups, low (0–7) and high (8–12), according to the expression level of JMJD6-ack375. Then the expression of JMJD6-ack375 in lung cancer was tested whether it was related to gender, age, differentiation degree, tumour size and TNM stage, respectively. **(C)** The expression of JMJD6-ack375 was examined in 68 lung cancer tissues with TNM stage I-II and stage III-IV. **(D)** JMJD6-ack375 expression was detected in 68 cases of tumor tissues with tumor size greater than or equal to 5 cm and less than 5 cm. **(E)** Kaplan-Meier analysis of JMJD6 hyperacetylation level, log-rank test, $P=0.022$. **(F)** The working model elucidates the molecular mechanism through which JMJD6 influences the expression of its downstream target METTL14 both pre- and post-acetylation, consequently impacting the expression of the ferroptosis-related protein SLC3A2. In this process, we demonstrated that acetylated JMJD6 enhances METTL14 expression by elevating H4R3me2a levels, whereas METTL14 overexpression suppresses SLC3A2 expression and impedes the progression of lung cancer cells by facilitating ferroptosis

Abbreviations

NSCLC	Non-small cell lung cancer
JMJD6	Jumonji domain-containing 6
METTL14	Methyltransferase-like 14
SLC3A2	Solute carrier family 3-member 2
GSH	γ -glutamyl cysteinyl + glycine
PCAF	P300/CBP-associated factor
CCRCC	Clear Cell Renal Cell Carcinoma
ANXA1	Annexin A1
DGAT1	Type I diacylglycerol acyltransferase
TKIs	Tyrosine kinase inhibitor
CRPC	Castration-resistant prostate cancer
U2AF65	The essential pre-mRNA splicing factor
YTHDC2	YTH domain containing 2
HOXA13	Homeobox A13
IGF2BP3	Insulin like growth factor 2 mRNA binding protein 3
STRIP2	Striatin-interacting protein 2
GCN5	General control non-depressible 5
SOX4	SRY-box transcription factor 4
MMP9	Matrix metalloproteinase-9
GPX4	Glutathione Peroxidase 4
HOXB9	Homeobox B9
NSUN2	NOP2/Sun RNA methyltransferase family member 2
NRF2	Nuclearrespiratory factor 2

Supplementary Information

The online version contains supplementary material available at <https://doi.org/10.1186/s12967-025-06241-8>.

Supplementary Material 1
Supplementary Material 2
Supplementary Material 3
Supplementary Material 4
Supplementary Material 5
Supplementary Material 6

Acknowledgements

We gratefully acknowledge the experimental animal center of Zhengzhou University for providing the necessary equipment for this study.

Author contributions

HXC and HYL conceived and designed the study. HXC and HYL performed most of the experiments and statistical analyses. NX, CXZ, YL and YL assisted in the experiments. XZZ, RKZ and LB collected clinical samples. QZK and JHW provided administrative, technical, or material support. HXC and HYL wrote the manuscript. All authors reviewed and edited the final manuscript. All authors read and approved the final manuscript.

Funding

This study was supported by grants from the National Natural Science Foundation of China (Grant No. 82173018), the Natural Science Foundation of Henan Province (Grant No. 232300421054), the National Natural Science Foundation of China (Grant No. 82370113), the Medical Science and

Technology Provincial and Ministerial Co-construction Project of Henan province (Grant No. SBGJ202102133, SBG202403034), the Young and Middle-aged Health Science and Technology Innovation Talents Project of Henan province (Grant No. YXKC2021036), the Funding for Scientific Research and Innovation Team of The First Affiliated Hospital of Zhengzhou University (Grant No. QNCXTD2023005), Henan Province Science and Technology Research and Development Joint Fund (Grant No. 242301420071), Zhengzhou University Education and Teaching Reform Research and Practice Project (Grant No. 2022ZZUJG298).

Data availability

All data that supporting the findings of this study are available from the corresponding author when requested.

Declarations

Ethics approval and consent to participate

This study was performed according to the ethical standards of the Declaration of Helsinki and received approval from the Ethics Committee at the First Affiliated Hospital of Zhengzhou University. Informed consent was obtained from all patients participating in this research.

Consent for publication

Not applicable.

Competing interests

The authors declare that they have no conflict of interest.

Author details

¹Department of Clinical Laboratory, The First Affiliated Hospital of Zhengzhou University, Zhengzhou, Henan, China

²Department of Obstetrics and Gynecology, The Third Affiliated Hospital of Zhengzhou University, Zhengzhou, Henan, China

³School of Life Science, Zhengzhou University, Zhengzhou, Henan, China

⁴Department of General Surgery, Zhecheng People's Hospital, Shangqiu, Henan, China

Received: 16 November 2024 / Accepted: 11 February 2025

Published online: 26 February 2025

References

1. Thai AA, Solomon BJ, Sequist LV, Gainor JF, Heist RS. Lung cancer. *Lancet*. 2021;398:535–54.
2. Leiter A, Veluswamy RR, Wisnivesky JP. The global burden of lung cancer: current status and future trends. *Nat Rev Clin Oncol*. 2023;20:624–39.
3. Sanaei MJ, Pourbagheri-Sigaroodi A, Rezvani A, Zabolli E, Salari S, Masjedi MR, Bashash D. Lung cancer vaccination from concept to reality: a critical review of clinical trials and latest advances. *Life Sci*. 2024;346:122652.
4. Xu J, Tian L, Qi W, Lv Q, Wang T. Advancements in NSCLC: from pathophysiological insights to targeted treatments. *Am J Clin Oncol*. 2024;47:291–303.
5. Dong RF, Zhu ML, Liu MM, Xu YT, Yuan LL, Bian J, Xia YZ, Kong LY. EGFR mutation mediates resistance to EGFR tyrosine kinase inhibitors in NSCLC: from molecular mechanisms to clinical research. *Pharmacol Res*. 2021;167:105583.
6. Kagamu H. Immunotherapy for non-small cell lung cancer. *Respir Investig*. 2024;62:307–12.

7. Yang Y, Wang J, Wang J, Zhao X, Zhang T, Yang Y, Pang J, Ou Q, Wu L, Xu X, et al. Unrevealing the therapeutic benefits of radiotherapy and consolidation immunotherapy using ctDNA-defined tumor clonality in unresectable locally advanced non-small cell lung cancer. *Cancer Lett.* 2024;582:216569.
8. Alduais Y, Zhang H, Fan F, Chen J, Chen B. Non-small cell lung cancer (NSCLC): a review of risk factors, diagnosis, and treatment. *Med (Baltim).* 2023;102:e32899.
9. Ren F, Fei Q, Qiu K, Zhang Y, Zhang H, Sun L. Liquid biopsy techniques and lung cancer: diagnosis, monitoring and evaluation. *J Exp Clin Cancer Res.* 2024;43:96.
10. Wang K, Yang C, Li H, Liu X, Zheng M, Xuan Z, Mei Z, Wang H. Role of the epigenetic modifier JMJD6 in Tumor Development and Regulation of Immune Response. *Front Immunol.* 2022;13:859893.
11. Cockman ME, Sugimoto Y, Pegg HB, Masson N, Salah E, Tumber A, Flynn HR, Kirkpatrick JM, Schofield CJ, Ratcliffe PJ. Widespread hydroxylation of unstructured lysine-rich protein domains by JMJD6. *Proc Natl Acad Sci U S A.* 2022;119:e2201483119.
12. Yang J, Chen S, Yang Y, Ma X, Shao B, Yang S, Wei Y, Wei X. Jumonji domain-containing protein 6 protein and its role in cancer. *Cell Prolif.* 2020;53:e12747.
13. Cioni B, Ratti S, Piva A, Tripodi I, Milani M, Menichetti F, Langella T, Botti L, De Cecco L, Chiodoni C, et al. JMJD6 shapes a Pro-tumor Microenvironment via ANXA1-Dependent macrophage polarization in breast Cancer. *Mol Cancer Res.* 2023;21:614–27.
14. Zhou J, Simon JM, Liao C, Zhang C, Hu L, Zurlo G, Liu X, Fan C, Hepperla A, Jia L, et al. An oncogenic JMJD6-DGAT1 axis tunes the epigenetic regulation of lipid droplet formation in clear cell renal cell carcinoma. *Mol Cell.* 2022;82:3030–e30443038.
15. Chen S, Wang M, Lu T, Liu Y, Hong W, He X, Cheng Y, Liu J, Wei Y, Wei X. JMJD6 in tumor-associated macrophage regulates macrophage polarization and cancer progression via STAT3/IL-10 axis. *Oncogene.* 2023;42:2737–50.
16. Li J, Cao F, Yin HL, Huang ZJ, Lin ZT, Mao N, Sun B, Wang G. Ferroptosis: past, present and future. *Cell Death Dis.* 2020;11:88.
17. Fotiadis D, Kanai Y, Palacin M. The SLC3 and SLC7 families of amino acid transporters. *Mol Aspects Med.* 2013;34:139–58.
18. Wang HH, Fan SQ, Zhan YT, Peng SP, Wang WY. Suppression of the SLC7A11/glutathione axis causes ferroptosis and apoptosis and alters the mitogen-activated protein kinase pathway in nasopharyngeal carcinoma. *Int J Biol Macromol.* 2024;254:127976.
19. Liang C, Zhang X, Yang M, Dong X. Recent progress in Ferroptosis Inducers for Cancer Therapy. *Adv Mater.* 2019;31:e1904197.
20. Liu MR, Zhu WT, Pei DS. System Xc(-): a key regulatory target of ferroptosis in cancer. *Invest New Drugs.* 2021;39:1123–31.
21. Koppula P, Zhang Y, Zhuang L, Gan B. Amino acid transporter SLC7A11/xCT at the crossroads of regulating redox homeostasis and nutrient dependency of cancer. *Cancer Commun (Lond).* 2018;38:12.
22. Rochette L, Dogon G, Rigal E, Zeller M, Cottin Y, Vergely C. Lipid peroxidation and iron metabolism: two corner stones in the homeostasis control of ferroptosis. *Int J Mol Sci.* 2022;24(1):449.
23. Chen Y, Jiang Z, Zhang C, Zhang L, Chen H, Xiao N, Bai L, Liu H, Wan J. 5-Methylcytosine transferase NSUN2 drives NRF2-mediated ferroptosis resistance in non-small cell lung cancer. *J Biol Chem.* 2024;300:106793.
24. Zhang W, Sun Y, Bai L, Zhi L, Yang Y, Zhao Q, et al. RBMS1 regulates lung cancer ferroptosis through translational control of SLC7A11. *J Clin Invest.* 2021;131(22):e152067.
25. Cai S, Zhang B, Huang C, Deng Y, Wang C, Yang Y, Xiang Z, Ni Y, Wang Z, Wang L, et al. CTRP6 protects against ferroptosis to drive lung cancer progression and metastasis by destabilizing SOCS2 and augmenting the xCT/GPX4 pathway. *Cancer Lett.* 2023;579:216465.
26. Liu X, Si W, Liu X, He L, Ren J, Yang Z, Yang J, Li W, Liu S, Pei F, et al. JMJD6 promotes melanoma carcinogenesis through regulation of the alternative splicing of PAK1, a key MAPK signaling component. *Mol Cancer.* 2017;16:175.
27. Wan J, Liu H, Yang L, Ma L, Liu J, Ming L. JMJD6 promotes hepatocellular carcinoma carcinogenesis by targeting CDK4. *Int J Cancer.* 2019;144:2489–500.
28. Zheng H, Tie Y, Fang Z, Wu X, Yi T, Huang S, Liang X, Qian Y, Wang X, Pi R, et al. Jumonji domain-containing 6 (JMJD6) identified as a potential therapeutic target in ovarian cancer. *Signal Transduct Target Ther.* 2019;4:24.
29. Pei R, Zhao L, Ding Y, Su Z, Li D, Zhu S, Xu L, Zhao W, Zhou W. JMJD6-BRD4 complex stimulates lncRNA HOTAIR transcription by binding to the promoter region of HOTAIR and induces radioresistance in liver cancer stem cells. *J Transl Med.* 2023;21:752.
30. Bentley AC. A survey of celiac-sprue patients: effect of dietary restrictions on religious practices. *J Gen Psychol.* 1988;115:7–14.
31. Yang F, Xiao Y, Ding JH, Jin X, Ma D, Li DQ, Shi JX, Huang W, Wang YP, Jiang YZ, Shao ZM. Ferroptosis heterogeneity in triple-negative breast cancer reveals an innovative immunotherapy combination strategy. *Cell Metab.* 2023;35:84–e100108.
32. Zhang Q, Deng T, Zhang H, Zuo D, Zhu Q, Bai M, Liu R, Ning T, Zhang L, Yu Z, et al. Adipocyte-derived exosomal MTTP suppresses ferroptosis and promotes Chemoresistance in Colorectal Cancer. *Adv Sci (Weinh).* 2022;9:e2203357.
33. Huang WM, Li ZX, Wu YH, Shi ZL, Mi JL, Hu K, Wang RS. m6A demethylase FTO renders radioresistance of nasopharyngeal carcinoma via promoting OTUB1-mediated anti-ferroptosis. *Transl Oncol.* 2023;27:101576.
34. Wang F, Sun Z, Zhang Q, Yang H, Yang G, Yang Q, Zhu Y, Wu W, Xu W, Wu X. Curdione induces ferroptosis mediated by m6A methylation via METTL14 and YTHDF2 in colorectal cancer. *Chin Med.* 2023;18:122.
35. Wysocka J, Allis CD, Coonrod S. Histone arginine methylation and its dynamic regulation. *Front Biosci.* 2006;11:344–55.
36. Yang Y, Lu Y, Espejo A, Wu J, Xu W, Liang S, Bedford MT. TDRD3 is an effector molecule for arginine-methylated histone marks. *Mol Cell.* 2010;40:1016–23.
37. Forde PM, Spicer J, Liu S, Provencio M, Mitsudomi T, Awad MM, Felip E, Broderick SR, Brahmer JR, Swanson SJ, et al. Neoadjuvant Nivolumab plus Chemotherapy in Resectable Lung Cancer. *N Engl J Med.* 2022;386:1973–85.
38. Pao W, Chmielecki J. Rational, biologically based treatment of EGFR-mutant non-small-cell lung cancer. *Nat Rev Cancer.* 2010;10:760–74.
39. Xiao RQ, Ran T, Huang QX, Hu GS, Fan DM, Yi J, Liu W. A specific JMJD6 inhibitor potentially suppresses multiple types of cancers both in vitro and in vivo. *Proc Natl Acad Sci U S A.* 2022;119:e2200753119.
40. Huang Y, Chen D, Liu C, Shen W, Ruan Y. Evolution and conservation of JmjC domain proteins in the green lineage. *Mol Genet Genomics.* 2016;291:33–49.
41. Aprelikova O, Chen K, El Touny LH, Brignatz-Guittard C, Han J, Qiu T, Yang HH, Lee MP, Zhu M, Green JE. The epigenetic modifier JMJD6 is amplified in mammary tumors and cooperates with c-Myc to enhance cellular transformation, tumor progression, and metastasis. *Clin Epigenetics.* 2016;8:38.
42. Rosager AM, Dahlrot RH, Sorensen MD, Bangso JA, Hansen S, Kristensen BW. The Epigenetic Regulator Jumonji Domain-Containing protein 6 (JMJD6) is highly expressed but not prognostic in IDH-Wildtype Glioblastoma patients. *J Neuropathol Exp Neurol.* 2022;81:54–60.
43. Tong D. Correction to: the role of JMJD6/U2AF65/AR-V7 axis in castration-resistant prostate cancer progression. *Cancer Cell Int.* 2021;21:301.
44. Ma L, Zhang X, Yu K, Xu X, Chen T, Shi Y, Wang Y, Qiu S, Guo S, Cui J, et al. Targeting SLC3A2 subunit of system X(C)(-) is essential for m(6)a reader YTHDC2 to be an endogenous ferroptosis inducer in lung adenocarcinoma. *Free Radic Biol Med.* 2021;168:25–43.
45. Xu X, Cui J, Wang H, Ma L, Zhang X, Guo W, Xue X, Wang Y, Qiu S, Tian X, et al. IGF2BP3 is an essential N(6)-methyladenosine biotarget for suppressing ferroptosis in lung adenocarcinoma cells. *Mater Today Bio.* 2022;17:100503.
46. Narita T, Weinert BT, Choudhary C. Functions and mechanisms of non-histone protein acetylation. *Nat Rev Mol Cell Biol.* 2019;20:156–74.
47. Zhang X, Chen Q, He Y, Shi Q, Yin C, Xie Y, Yu H, Bao Y, Wang X, Tang C, Dong Z. STRIP2 motivates non-small cell lung cancer progression by modulating the TMBIM6 stability through IGF2BP3 dependent. *J Exp Clin Cancer Res.* 2023;42:19.
48. Ge W, Gong Y, Li Y, Wu N, Ruan Y, Xu T, Shu Y, Qiu W, Wang Y, Zhao C. IL-17 induces non-small cell lung cancer metastasis via GCN5-dependent SOX4 acetylation enhancing MMP9 gene transcription and expression. *Mol Carcinog.* 2023;62:1399–416.
49. Wan J, Xu W, Zhan J, Ma J, Li X, Xie Y, Wang J, Zhu WG, Luo J, Zhang H. PCAF-mediated acetylation of transcriptional factor HOXB9 suppresses lung adenocarcinoma progression by targeting oncogenic protein JMJD6. *Nucleic Acids Res.* 2016;44:10662–75.

Publisher's note

Springer Nature remains neutral with regard to jurisdictional claims in published maps and institutional affiliations.